Table 2. Number of Lactose Molecules and Lactose Density on Gold Nanoparticles

	lac25	lac50
number of lactose molecules on a single particle[a]	130	260
area occupied by a single lactose molecule (nm^2)[b]	26.8	13.4
average distance between lactose moieties (nm)[c]	5.18	3.66

[a] Calculated from the number of PEG chains on a single gold nanoparticle (520 chains/particle) and the lactose functionality. [b] The surface area of PEGylated gold nanoparticles [$4\pi \times (33.3/2)^2$ 3.48×10^3 nm^2] was divided by the number of lactose molecules on a single gold nanoparticle. [c] Square root of the area occupied by one lactose molecule.

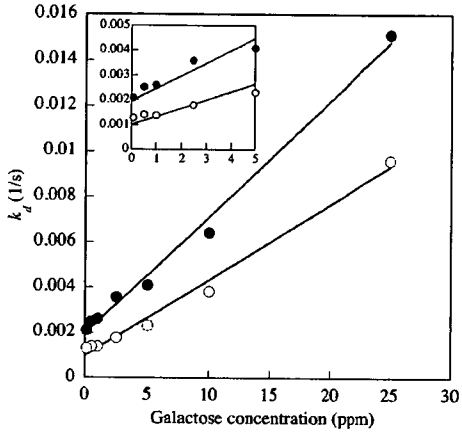

Figure 5. The relationship of the dissociation rate constant (k_d) to the injected galactose concentration. The k_d was obtained by curve fitting of the sensorgrams in Figure 4 as described in the Experimental Section. Closed circles indicate k_d of lac25 ($R^2 = 0.9924$, $\chi^2 = 3.83$), and open circles indicate k_d of lac50 ($R^2 = 0.9895$, $\chi^2 = 1.95$). The insert is the expanded figure in the range 0−5 ppm galactose.

half of the average distance between two RCA_{120} molecules on the sensor chip surface.

3.4. Colloidal Au Replacement Assay. The SPR signal enhancement by the lactosyl-PEGylated gold nanoparticles was then applied to the direct and quantitative detection of the LMW analyte, galactose. The novel method developed here (colloidal Au replacement assay) is based on the elution of the preadsorbed lactosyl-PEGylated gold nanoparticles from the sensor chip surface due to the substitution with galactose in the solution. A practical advantage of this method is that it does not require any labeling of the LMW analytes. The lactosyl-PEGylated gold nanoparticles (ca. 900−1300 RU) were initially adsorbed on the RCA_{120}-immobilized CM3 sensor chip. Free galactose, in varying concentrations (0.1−100 ppm), was then injected into the flow cell. During the elution phase of each sensorgram, the response level was normalized by the amount of the preadsorbed PEGylated gold nanoparticles as shown in Figure 4 (relative response) (*12*, *13*). Obviously, the elution of the gold nanoparticles correlated with the galactose concentration. To quantify the degree of galactose-induced dissociation, the dissociation rate constant (k_d) was calculated by curve fitting against the dissociation sensorgrams. Notably, the k_d has a linear relationship in the 0.1−25 ppm galactose concentration range for both lac25 and lac50 (Figure 5), thus permitting the quantitative analysis of galactose. Moreover, a decrease in the relative response fits nicely to a linear relationship with the galactose concentration for both lac25 (Figure 6A) and lac50 (Figure 6B) measured at several time points. As seen in the inserts of Figure 6A,B, a quantitative analysis is feasible from 0.1 to 50 ppm, indicating the significantly high sensitivity of this method. It is also noted that the linearity was valid for an appreciably wide

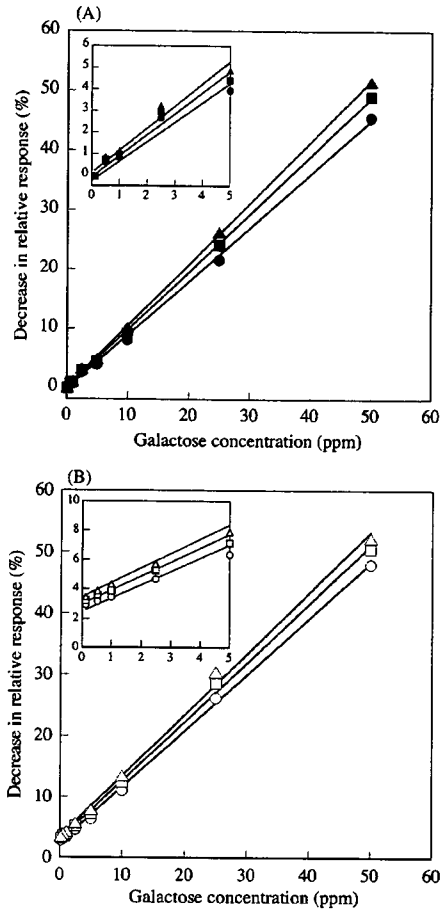

Figure 6. Relationship of the decrease in the relative response vs injected galactose concentration. All the plots in these figures were obtained by the subtraction of the relative response recorded under galactose-induced dissociation from the relative response recorded under only the running buffer. A linear response to the galactose concentration (0.1−50 ppm) was observed in all the plots ($R^2 > 0.997$). The inserts are the expanded figures in the range 0−5 ppm galactose. (A) Closed circles, squares, and triangles are the data corresponding to the time points at 25, 30, and 35 s in the sensorgrams of the lac25 elution (Figure 4a), respectively. (B) Open circles, squares, and triangles are the data points corresponding to the times of 50, 60, and 70 s in the sensorgrams of the lac50 elution (Figure 4b), respectively.

range of response times: 20−30 s for lac25 and 50−70 s for lac50. This linearity in the decrease of the relative response reveals a practical advantage of the colloidal Au replacement assay. Note that the colloidal Au replacement assay achieves a sensitivity comparable to that of ELISA in a much shorter operating time (~5 min) without any cumbersome processes of multiple washing and separation steps, which are necessary for the ELISA assay.

This method may be applicable for the quantitative sensing of various LMW compounds of practical interest, including sugars (*18*, *19*), by utilizing an appropriate combination of analyte-installed PEGylated gold nanoparticles and immobilized ligands to construct a high-throughput screening system.

4. CONCLUSION

PEGylated gold nanoparticles with different lactose functionalities (0−50%) on the distal end of PEG were prepared in order to construct a novel method for the quantitative assay of LMW analytes by SPR (colloidal Au replacement assay). The lactosyl-PEGylated gold nanoparticles showed a specific adsorption on the sensor chip surface bearing the RCA_{120} lectin,

dependent on the lactose functionality on the surface of the gold nanoparticles due to the multivalent interaction of the nanoparticles with RCA_{120} immobilized on the sensor chip. Interestingly, preadsorbed lactosyl-PEGylated gold nanoparticles on the RCA_{120}-immobilized sensor chip were eluted from the sensor chip by the injection of galactose, in a manner proportional to the galactose concentration. Eventually, this method allowed for the quantitative assay over a wide range of galactose concentrations (0.1−50 ppm) within a short operating time (~5 min). This concept of colloidal Au replacement assay would be applicable to the highly sensitive SPR quantification of various LMW analytes.

ACKNOWLEDGMENT

The authors acknowledge Dr. Eduardo Jule, the University of Tokyo, for his advice about the SPR experiments. This study was financially supported by Special Coordination Funds for Promoting Science and Technology from the Ministry of Education, Culture, Sports, Science and Technology of Japan (MEXT) as well as by the Core Research for Evolutional Science and Technology (CREST) from the Japan Science and Technology Agency (JST) and also by a Grant for the 21st Century COE Program "Human-Friendly Materials based on Chemistry" from MEXT. S.T. would like to express his special gratitude for the scholarship from the Asahi Glass Scholarship Foundation.

Supporting Information Available: Sensorgrams for the curve fitting of lac25 and lac50. This material is available free of charge via the Internet at http://pubs.acs.org/BC.

LITERATURE CITED

(1) Liedberg, B., Nylander, C., and Lundström, I. (1983) Surface plasmon resonance for gas detection and biosensing. *Biosensors and Actuators 4*, 299−304.

(2) Karlsson, R., Michaelsson, A., and Mattsson, L. (1991) Kinetic analysis of monoclonal antibody-antigen interactions with a new biosensor based analytical system. *J. Immunol. Methods 145*, 229−240.

(3) Homola, J., Yee, S. S., and Gauglitz, G. (1999) Surface plasmon resonance sensors: review. *Sens. and Actuators, B 54*, 3−15.

(4) Tawa, K., and Knoll, W. (2004) Mismatching base-pair dependence of the kinetics of DNA-DNA hybridization studied by surface plasmon fluorescence spectroscopy. *Nucleic Acids Res. 32*, 2372−2377.

(5) Lyon, L. A., Musick, M. D., and Natan, M. J. (1998) Colloidal Au-enhanced surface plasmon immunosensing. *Anal. Chem. 70*, 5177−5183.

(6) He, L., Musick, M. D., Nicewarner, S. R., Salinas, F. G., Benkovic, S. J., Natan, M. J., and Keating, C. D. (2000) Colloidal Au-enhanced surface plasmon resonance for ultrasensitive detection of DNA hybridization. *J. Am. Chem. Soc. 122*, 9071−9077.

(7) Hutter, E., Cha, S., Liu, J-F., Park, J., Yi, J., Fendler, J. H., and Roy, D. (2001) Role of substrate metal in gold nanoparticle enhanced surface plasmon resonance imaging. *J. Phys. Chem. B 105*, 8−12.

(8) Akiyama, Y., Otsuka, H., Nagasaki, Y., Kato, M., and Kataoka, K. (2000) Selective synthesis of heterobifunctional poly(ethylene glycol) derivatives containing both mercapto and acetal terminals. *Bioconjugate Chem. 11*, 947−950.

(9) Otsuka, H., Akiyama, Y., Nagasaki, Y., and Kataoka, K. (2001) Quantitative and reversible lectin-induced association of gold nanoparticles modified with α-lactosyl-ω-mercapto-poly(ethylene glycol). *J. Am. Chem. Soc. 123*, 8226−8230.

(10) Takae, S., Akiyama, Y., Otsuka, H., Nakamura, T., Nagasaki, Y., and Kataoka, K. (2005) Ligand density effect on biorecognition by PEGylated gold nanoparticles: regulated interaction of RCA_{120} lectin with lactose installed to the distal end of tethered PEG strands on gold surface. *Biomacromolecules 6*, 818−824.

(11) Stenberg, E., Persson, B., Roos, H., and Urbaniczky, C. (1991) Quantitative determination of surface concentration of protein with surface plasmon resonance using radiolabeled proteins. *J. Colloid Interface Sci. 143*, 513−526.

(12) Suzuki, F., Goto, M., Sawa, C., Ito, S., Watanabe, H., Sawada, J., and Handa, H. (1998) Functional interaction of transcription factor human GA-binding protein subunits. *J. Biol. Chem. 273*, 29302−29308.

(13) Murai, N., Taguchi, H., and Yoshida, M. (1995) Kinetic analysis of interactions between GroEL and reduced α-lactalbumin. *J. Biol. Chem. 270*, 19957−19963.

(14) Dooley, T. P., and Houston, L. L. (1982) Binding of two molecules of 4-methylumbelliferyl galactose or 4-methylumbelliferyl N-acetylgalactosamine to the B chains of ricin and ricinus communis agglutinin and to purified ricin B chain. *J. Biol. Chem. 257*, 4147−4151.

(15) Jule, E., Nagasaki, Y., and Kataoka, K. (2003) Lactose-installed poly(ethylene glycol)-poly(D,L-lactide) block copolymer micelles exhibit fast-rate binding and high affinity toward a protein bed simulating a cell surface. A surface plasmon resonance study. *Bioconjugate Chem. 14*, 177−186.

(16) Lin, C., Yeh, Y., Yang, C., Chen, G., Chen, Y., Wu, Y., and Chen, C. (2003) Quantitative analysis of multivalent interactions of carbohydrate-encapsulated gold nanoparticles with concanavalin A. *Chem. Commun.* 2920−2921.

(17) Hernaiz, M. J., de la Fuente, J. M., Barrientos, A. G., and Penades, S. (2002) A model system mimicking glycophingolipid clusters to quantify carbohydrate self-interaction by surface plasmon resonance. *Angew. Chem., Int. Ed. 41*, 1554−1557.

(18) Park, S., Boo, H., and Chung, T. D. (2006) Electrochemical non-enzymatic glucose sensors. *Anal. Chim. Acta 556*, 46−57.

(19) Perez-Olmos, R., Soto, J. C., Zarate, N., Araujo, A. N., Lima, J. L. F. C., and Saraiva, M. L. M. F. S. (2005) Application of sequential injection analysis (SIA) to food analysis. *Food Chem. 90*, 471−490.

BC0603541

Available online at www.sciencedirect.com
ScienceDirect
Journal of Controlled Release 121 (2007) 38–48
journal of controlled release
www.elsevier.com/locate/jconrel

Transfection study using multicellular tumor spheroids for screening non-viral polymeric gene vectors with low cytotoxicity and high transfection efficiencies

Muri Han [a], Younsoo Bae [b,c], Nobuhiro Nishiyama [b,c,d], Kanjiro Miyata [c,e], Makoto Oba [f], Kazunori Kataoka [a,b,c,d,e,*]

[a] Department of Materials Engineering, School of Engineering, The University of Tokyo, 7-3-1 Hongo, Bunkyo-ku, Tokyo 113-8656, Japan
[b] Center for Disease Biology and Integrative Medicine, School of Medicine, The University of Tokyo, 7-3-1 Hongo, Bunkyo-ku, Tokyo 113-0033, Japan
[c] Center for NanoBio Integration, The University of Tokyo, 7-3-1 Hongo, Bunkyo-ku, Tokyo 113-8656, Japan
[d] Core Research for Evolutional Science and Technology (CREST), Japan Science and Technology Agency (JST), Japan
[e] Department of Bioengineering, School of Engineering, The University of Tokyo, 7-3-1 Hongo, Bunkyo-ku, Tokyo 113-0033, Japan
[f] Department of Clinical Vascular Regeneration, School of Medicine, The University of Tokyo, 7-3-1 Hongo, Bunkyo-ku, Tokyo 113-8655, Japan

Received 19 March 2007; accepted 8 May 2007
Available online 17 May 2007

Abstract

Polyplexes consisting of plasmid DNA and polycations have received much attention as promising vectors for gene transfer. For effective gene therapy, polycations with different polyamine structures in the side chain were developed to ensure their buffering capacity for endosomal escape, and their PEGylated block copolymers were developed to increase their stability and biocompatibility. The effects of the chemical structures of polycations and their PEGylation on transfection and cytotoxicity were elucidated by use of a three-dimensional multicellular tumor spheroid of human hepatoma HuH-7 cells. Various features of transfection with polyplex micelles, which have been hard to observe in conventional monolayer cultures, were revealed by the multicellular tumor spheroid (MCTS) model in terms of cytotoxicity and time-dependent behaviors of transfected gene expression under three-dimensional microenvironments. By using this system, the polyplex micelle from poly(ethylene glycol)-*b*-poly(*N*-substituted asparagine) copolymers having the *N*-(2-aminoethyl)-2-aminoethyl group in the side chain (PEG-*b*-P[Asp(DET)] polyplex micelle) was proved to achieve high transfection efficiencies as well as low cytotoxicity, both of which are critical properties for successful in vivo gene delivery.

Keywords: Non-viral gene vector; Block copolymer; Polyplex micelle; Spheroid

1. Introduction

A variety of non-viral polymeric gene vectors have received much attention in the past decade [1–3] for the delivery of genetic materials to the targeted cells in an effective and safe manner. Especially, the polyplexes formed by the electrostatic interaction between plasmid DNA (pDNA) and polycations have been designed to condense pDNA by shielding its negative charges, protect pDNA from rapid nucleolytic degradation, and facilitate its cellular uptake in order to achieve effective gene delivery [4–6]. It is well known that the chemical structures of polycations in polyplex systems play important roles in transfection efficiency. In this regard, polyethylenimine (PEI)-based polyplexes have been shown to be highly transfectable, presumably through the buffering of the endosomal cavity (i.e., so-called proton sponge effect) [2]. One of the advantages of polyplex systems is the possibility of various structural modifications to improve the stability and transfection efficiency of the polyplexes. Among such modifications, PEGylation [modification with poly(ethylene glycol)(PEG)] of polycations is a promising way to realize systemic gene delivery due to the improved stability of polyplexes in biological media [7–10].

* Corresponding author. Department of Materials Engineering, Graduate School of Engineering, The University of Tokyo, 7-3-1 Hongo, Bunkyo-ku, Tokyo 113-8656, Japan. Fax: +81 3 5841 7139.
E-mail address: kataoka@bmw.t.u-tokyo.ac.jp (K. Kataoka).

0168-3659/$ - see front matter © 2007 Elsevier B.V. All rights reserved.
doi:10.1016/j.jconrel.2007.05.012

A typical PEGylated polyplex is a core-shell type polyplex (polyplex micelle) formed through the electrostatic interaction between pDNA and PEG-*block*-polycation copolymers. Polyplex micelles have been demonstrated to show high colloidal stability under biological media and substantial transfection activity against various cells even after preincubation with serum proteins [11,12]. Moreover, polyplex micelles showed prolonged blood circulation and in vivo gene transfer to liver [5,13]. The chemical structures of polycations in block copolymers substantially affect the capability of polyplexes as efficient gene vectors. In this regard, we recently reported the development of highly transfectable but remarkably low cytotoxic PEG-*block*-polycation copolymers: PEG-*b*-poly(*N*-substituted asparagine) copolymers having the *N*-(2-aminoethyl)-2-aminoethyl group in the side chain (PEG-*b*-P[Asp(DET)]) [14]. Polyplex micelles from PEG-*b*-P[Asp(DET)] showed efficient and non-toxic transfection to several primary cells including endothelial and smooth muscle cells, which are sensitive to the polyplex-induced cytotoxicity, and successful gene transfection in vivo to vascular lesions [15]. Thus, the PEG-*b*-P[Asp(DET)] polyplex micelle is expected to be a potent non-viral vector for in vivo gene delivery.

The unique feature of the PEG-*b*-P[Asp(DET)] polyplex micelle to achieve appreciably high transfection efficacy with substantially lowered toxicity motivated us to further clarify the effects of PEGylation and the chemical structures of polyasparagine-based polyplexes on their transfection and cytotoxic behaviors. For this purpose, we have compared here two types of polyasparagine-based polycations having a subtle difference in the number of methylene units in the side chain: *N*-(2-aminoethyl)-2-aminoethyl group (P[Asp(DET)]) and *N*-(3-aminopropyl)-3-aminopropyl group (P[Asp(DPT)]). Furthermore, to explore the effect of PEGylation on polyplex behavior, two types of PEG-*b*-cationic polyasparagines, PEG-*b*-P[Asp(DET)] and PEG-*b*-P[Asp(DPT)], were prepared for the construction of polyplex micelles (Scheme 1). The transfection activity and cytotoxicity of polyplexes and polyplex micelles were evaluated with multicellular tumor spheroids (MCTS) as well as conventional monolayer culture cells. We focus on MCTS here because they are known to be very useful three-dimensional in vitro tumor models, representing morphological and functional features of in vivo avascular solid tumors, and because they are characterized by prolonged viable spans with actively proliferating outer cell layers [16]. Recently, Mellor et al. applied the transfection of polyethylenimine-based polyplexes to the MCTS with the relatively large size (~474 μm) to assess the penetration of the polyplexes inside the spheroids, approaching the issue of polyplex percolation in actual in vivo tissues [17]. In the present study, we focused on the MCTS with the relatively small size due to our finding that the size of MCTS is highly sensitive to polyplex-induced cytotoxicity; MCTS of approximately 100 μm showed even higher sensitivity than monolayered culture cells, probably due to their immature development of cell–cell and cell–extracellular matrix (ECM) interactions. Worth noting is that the prolonged viable span of MCTS allowed long-term evaluation of more than 10 days of the expression of transfected genes. These properties of MCTS models enabled us to evaluate polyplex systems under conditions close to those of in vivo solid tumors, revealing the excellent biocompatibility and durable gene expression behaviors of PEG-*b*-P[Asp(DET)] polyplex micelles.

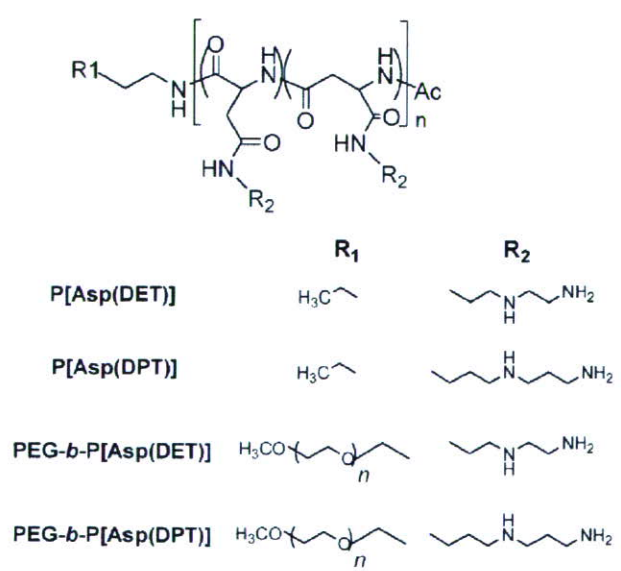

Scheme 1. Chemical structures of polycations.

2. Experimental

2.1. Materials

β-Benzyl-L-aspartate *N*-carboxyanhidride (BLA-NCA) and α-methoxy-ω-amino poly(ethylene glycol) (MeO-PEG-NH_2) (M_r=12,000) were obtained from Nippon Oil and Fats Co., Ltd. (Japan). Diethylenetriaimine (DET) and dipropylenetriamine (DPT) were purchased from Tokyo Kasei Kogyo Co., Ltd. (Japan) and distilled over CaH_2 under reduced pressure. *N,N*-Dimethylformamide (DMF), dichloromethane, and acetic anhydride were purchased from Wako Pure Chemical Industries, Ltd. (Japan) and purified by general methods before use. Linear polyethylenimine (ExGen 500 in vitro transfection reagent, 22 KDa) and branched polyethylenimine (25 KDa) were purchased from Fermentas (Canada) and Aldrich (USA), respectively.

2.2. Synthesis of poly(N-substituted asparagines) and their block copolymers with poly(ethylene glycol) (PEG)

The PEG-*block*-poly(β-benzyl L-aspartate) (PEG-*b*-PBLA) was prepared as previously reported [14]. Briefly, BLA-NCA was polymerized in DMF at 40 °C from the terminal primary amino group of MeO-PEG-NH_2, followed by the acetylation of the *N*-terminus of PBLA by acetic anhydride to obtain PEG-*b*-PBLA-Ac. PEG-*b*-PBLA-Ac was confirmed to have a unimodal molecular weight distribution (M_w/M_n: 1.17) by gel-permeation chromatography (GPC) measurement [columns: TSK-gel G4000HHR+G3000HHR, eluent: DMF+10 mM LiCl, T=40 °C, detector: Refractive Index (RI)] (data not shown).

The degree of polymerization (DP) of PBLA was calculated to be 101 based on ^{1}H NMR spectroscopy (data not shown).

Lyophilized PEG-*b*-PBLA (300 mg, 11.6 μmol) was dissolved in DMF (10 mL), followed by the reaction with DET (50 equiv to benzyl group of PBLA segment, 4.0 g, 39.4 mmol) under mild anhydrous conditions to obtain PEG-*b*-P[Asp(DET)]. After 24 h, the reaction mixture was slowly added dropwise into a solution of acetic acid (10% *v/v*, 40 mL) and dialyzed against a solution of 0.01 N HCl and then distilled water (M_r cutoff: 3500 Da). The final solution was lyophilized to obtain the polymer as the chloride salt form, and the yield was approximately 90%. Similarly, PEG-*b*-P[Asp(DPT)] was synthesized by the aminolysis reaction of PEG-*b*-PBLA-Ac with DPT. The structures of these block catiomers were confirmed by ^{1}H and ^{13}C NMR measurements.

Cationic homopolymers, P[Asp(DET)] and P[Asp(DPT)], were synthesized by the aminolysis reaction of PBLA homopolymer [degree of polymerization (DP): 98], which was obtained by the polymerization of BLA-NCA initiated by *n*-butylamine. The unimodal distribution and the almost 100% conversion of the BLA side chains of these homopolymers into the desired amino groups were confirmed by GPC and ^{1}H NMR measurements, respectively.

2.3. Titration of polymers

Each homopolymer (68 mg of P[Asp(DET)] and 75 mg of P[Asp(DPT)]) or block copolymer (98 mg of PEG-*b*-P[Asp(DET)] and 104 mg of PEG-*b*-P[Asp(DPT)]) was dissolved in 40 mL of 0.005 N HCl with 150 mM NaCl, and titrated with 0.05 N NaOH with 150 mM NaCl at 37 °C. An automatic titrator (TITSTATION TS-2000, Hiranuma Co., Ltd., Kyoto, Japan) was used for the titration. In this experiment, the titrant was added in 0.0315 mL quantities after the confirmation that the pH values became stable (minimal interval: 30 s). The pH-α curves were determined from the obtained titration curve. For the estimation of the charge in the protonation affinity with α apparent pK(=pH+log[α/(1−α)]) was plotted against 1−α, where K is the effective dissociation constant.

2.4. Plasmid DNA

The plasmid, pCAcc vector having CAG promoter [18], was provided by RIKEN Bioresource Center (Japan). Also, a fragment cDNA of SEYFP-F46L (*Venus*), which is a variant of yellow fluorescent protein with the mutation F46L [19], was provided by Dr. A. Miyawaki at the Brain Science Institute, RIKEN (Japan) and inserted into the pCAcc vector (pCAcc+*Venus*). Each plasmid DNA (pDNA) was amplified in competent DH5α *Escherichia coli* and purified using HiSpeed Plasmid MaxiKit (QIAGEN Sciences Co., Inc., Germany). The pDNA concentration was determined by the absorption at 260 nm.

2.5. Preparation of the polyplexes

Poly(ethylene glycol)-*block*-polycation copolymer and pDNA were first separately dissolved in 10 mM Tris–HCl buffer (pH 7.4). Then, both solutions were mixed at various ratios of the number of amino group (primary and secondary amino groups) units per nucleotide (*N/P* ratios). The final pDNA concentration of the mixture was adjusted to 100 μg/mL. Polyplex micelle was applied to each well for transfection after overnight incubation at ambient temperature. Polyplex was prepared similarly by mixing cationic homopolymer and pDNA solution. Polyplex was applied to each well for transfection after 30 min of incubation at ambient temperature.

2.6. In vitro transfection to HuH-7 cells

For the monolayer culture study, human hepatoma HuH-7 cells were seeded on 24-well culture plates and incubated overnight in 400 μL of Dulbecco's modified eagle's medium (DMEM) containing 10% fetal bovine serum (FBS) before transfection. Then, 10 μL of each polyplex solution was applied to each well for the transfection. The amount of pDNA was adjusted to 1 μg per well. After 24 h of incubation, the medium was replaced with 400 μL of the medium containing 10% serum, followed by an additional 24 h of incubation. The luciferase gene expression was then evaluated using the Luciferase Assay System (Promega, USA) and a Lumat LB9507 luminometer (Berthold Technologies, Germany). The amount of protein in each well was concomitantly determined using a Micro BCA Protein Assay Reagent Kit. To prepare MCTS, 200 μL of cell suspension (2×10^2 cell/ml) was seeded into a 96-well culture plate designed for spheroid formation (SUMILONCELLTIGHT, Sumitomo Bakelite Co., Ltd., Japan). After 48 h of incubation, a multicellular spheroid with diameter of ca 100 μm was spontaneously formed in each well. Then, 10 μL of each polyplex solution was applied to each well for the transfection. The amount of pDNA was adjusted to 1 μg per well. After 24 h of incubation, the medium was replaced with 200 μL of the medium containing 10% serum, followed by an additional 24 h of incubation. During the incubation period, the medium was replaced by fresh medium containing 10% serum every 3 days. The *Venus* gene expression was then evaluated using an LSM 510 confocal microscope (Carl Zeiss, Germany; excitation wavelength: 488 nm).

2.7. Live/dead assay

Live and Dead assay was accomplished with the Live/Dead kit protocol (Molecular Probes, USA) against cultured spheroids. Spheroids were rinsed with PBS (−) and then incubated with a solution containing 0.8 μM calcein AM (excitation 495 nm, emission 515 nm) and 4 μM EthD-1 (excitation 495 nm, emission 635 nm) in PBS (−) for 3 h at 37 °C, followed by observation through a Carl Zeiss LSM 510 confocal laser scanning microscope. The concentration and incubation time were optimized to allow the selective labeling of HuH-7 spheroids between live and dead cells.

2.8. Fluorescence measurements

For observation of the gene expression of the fluorescent protein *Venus*, MCTS samples were rinsed and mounted in PBS (−), and then observed by confocal microscope. The LSM 510

laser scanning microscope was used for the optical sectioning of the spheroids. An argon gas laser with an excitation wavelength of 488 nm was used to emit the fluorescence of the YFP.

2.9. Cell viability assay

Cell viability assay was accomplished with a protocol (CellTiter-Glo®Luminescent Cell Viability Assay, Promega, USA) against cultured cells. After 24 h incubation of HuH-7 cells in opaque 24-well plates, the polyplex to be tested was added. The cells were rinsed with PBS (−) after 24 h of incubation, then 200 μL of reagent to an equal volume of cell culture medium was added to each well. After mixing for 2 min, the plate was incubated at room temperature for 10 min. The luminescence was evaluated using a Lumat LB9507 luminometer (Berthold Technologies, Germany).

2.10. Quantification of gene expression in MCTS

The total intensity was calculated from the piled up fluorescence images of fluorescence of *Venus* from each optical slice (at a depth of 1 μm) by Imaris® software in combination with Imaris MeasurementPro (Carl Zeiss, Germany), which enables the measurement of the intensity value for groups of selected voxels. The relative intensity was determined from the total intensity of one spheroid divided by a volume of spheroid.

2.11. Dissociation of P[Asp(DET)] polyplex and PEG-b-P[Asp(DET)] micelle

The release of pDNA from the complexes was evaluated through the exchange reaction with an anionic lipid, 1,2-dioleoyl-*sn*-glycero-3-phospho-L-serine sodium salt (DOPS, Sigma). Two mg/mL of DOPS solution was added to the P[Asp(DET)] polyplex and to the PEG-*b*-P[Asp(DET)] polyplex micelle solutions prepared at the *N/P* ratio of 20 to obtain mixed solutions with varying unit molar ratios ([carboxyl groups in DOPS]/[phosphate groups in pDNA]). The final pDNA concentration was adjusted to 16.7 μg/mL. After overnight incubation at 25 °C, the mixed solutions were electrophoresed with 0.9 wt.% agarose gel in the buffer (3.3 mM Tris–acetic acid (pH 7.4)+1.7 mM sodium acetate+1 mM EDTA2Na). pDNAs in the gel were visualized by soaking the gel in an ethidium bromide solution (0.5 mg/L) and analyzed using a Luminous Imager V5 (AISIN SEIKI Co., Ltd., Japan).

3. Results

3.1. Protonation behaviors of polycations and their block copolymers with PEG

In this study, sets of cationic poly(*N*-substituted asparagine) homopolymers and PEG-*b*-poly(*N*-substituted asparagine) copolymers having the *N*-(2-aminoethyl)-2-aminoethyl group (P[Asp(DET)]) or the *N*-(3-aminopropyl)-3-aminopropyl group (P[Asp(DPT)]) in the side chain (Scheme 1) were prepared to study the effects of the chemical structures of polycations as well as the PEGylation of polycations on the properties of polyplex components. This synthetic method is based on our finding that the flanking benzyl ester groups of PBLA undergo a quantitative aminolysis reaction with various polyamine compounds under careful anhydrous conditions, so that a series of polymers has the same polymerization degree and distribution [14], allowing a direct comparison of subtle changes in their chemical structures.

The pH-dependent protonation behaviors of the obtained homopolymers, P[Asp(DET)] and P[Asp(DPT)], in 150 mM NaCl-containing media at 37°C seemed to be clearly distinct as shown in Fig. 1A. Indeed, P[Asp(DET)] displayed two-step protonation behavior and the protonation degree (α) of 0.53 at pH 7.4, whereas the protonation of P[Asp(DPT)] did not show clear two-step protonation and showed a higher protonation degree (α=0.88) at pH 7.4. From the p*K*–α curve (data not shown), the pK_1 (p*K* at α=0.25) and pK_2 (p*K* at α=0.75) of P[Asp(DET)] were calculated as 9.1 and 6.3, respectively, and the pK_1 and pK_2 of P[Asp(DPT)] were also calculated as 9.7 and 8.6, respectively. The two distinct p*K* values (pK_1 and pK_2) correspond to the first and

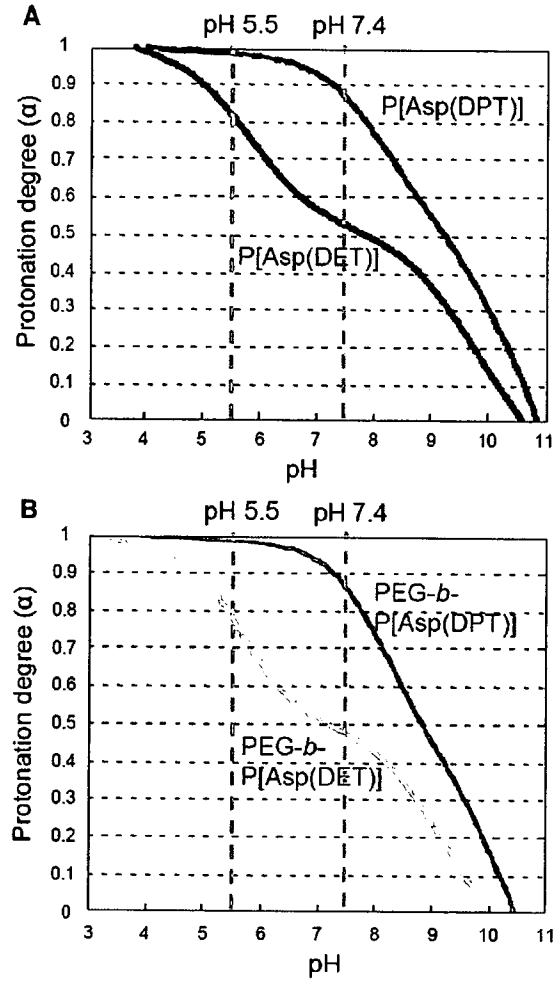

Fig. 1. pH–α (protonation degree) curves of P[Asp(DET)] and P[Asp(DPT)] (A) and PEG-*b*-P[Asp(DET)] and PEG-*b*-P[Asp(DPT)] (B) (37 °C, 150 mM NaCl, 0.05 M NaOH as titrant, 0.5 mmol amine concentration).

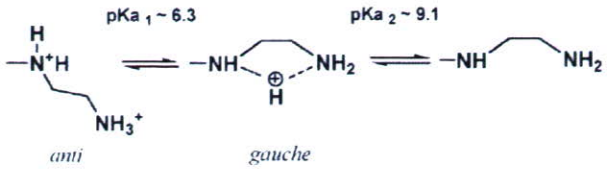

Scheme 2. Two-step protonation of ethylenediamine side chain of P[Asp(DET)].

second protonation steps of diamine units, respectively, in the side chain. Consequently, P[Asp(DET)] might exert a substantial buffering capacity in the pH range from 7.4 to 5.0, leading presumably to potent transfection activity based on the proton sponge effect. It is noteworthy that P[Asp(DET)] has a two orders of magnitude higher proton dissociation constant (or lower protonation constant) for the second protonation than P[Asp(DPT)], indicating that the former is less favorable than the latter to the double-protonated state. This may be due to the strong electrostatic repulsion between two protonated amines in ethylenediamine units of P[Asp(DET)] to take only the *anti*-conformation (Scheme 2). As seen in the case of P[Asp(DPT)], an increase in one more unit of the methylene group between two amino groups in the side chain effectively reduces the electrostatic repulsion to facilitate the protonation.

pH-α curves of PEG-*b*-poly(*N*-substituted asparagine) (PEG-*b*-P[Asp(DET)] and PEG-*b*-P[Asp(DPT)]) were also shown in Fig. 1B, showing a tendency similar to those of the homopolymers in Fig. 1A. From these results, the pK_1 and pK_2 of PEG-*b*-P[Asp(DET)] were calculated as 8.5 and 6.2, whereas the pK_1 and pK_2 of PEG-*b*-P[Asp(DPT)] were calculated as 9.3 and 8.5, respectively. It is noted that PEGylation of the polycations decreased the p*K* values, suggesting that PEGylation might prevent the protonation of polycations. Presumably, this might be explained by the decrease in the local permittivity of polycations caused by surrounding PEG chains.

3.2. Transfection efficiencies and cytotoxicity of polyplexes against monolayer cultured cells

The transfection efficiencies of cationic homopolymers/pDNA polyplexes against monolayer cultured HuH-7 cells were evaluated. The results of transfection after 48 h incubation (24 h incubation with the polyplexes followed by 24 h post-incubation after medium replacement) are shown in Fig. 2A. P[Asp(DET)] polyplexes showed high transfection efficiencies over the range of *N*/*P* ratios tested in this study. Especially, they displayed comparable or even higher transfection efficiencies at *N*/*P*=20 and 40 compared with LPEI and BPEI polyplexes [*N*/*P*=6 for LPEI according to the manufacturer's recommendation and *N*/*P*=10 for BPEI by optimization], which have been widely used in experimental transfection. P[Asp(DPT)] polyplexes showed appreciable transfection efficiency at *N*/*P*=10; however, the efficiency decreased at *N*/*P*=20 and 40, probably due to the emergence of significant cytotoxicity (Fig. 3).

Regarding the cytotoxicity of the polyplexes from cationic homopolymers (Fig. 3), both LPEI and BPEI polyplexes induced significant decreases in cell viability even at the *N*/*P* ratio appropriate for transfection. Polyplexes from P[Asp(DET)] were significantly less cytotoxic than the other polyplexes, whereas P[Asp(DPT)] polyplexes turned out to be highly cytotoxic. Thus, a subtle change in the chemical structure of the side chain of poly(*N*-substituted asparagine) unprecedentedly affected the cytotoxicity of the polyplexes.

In the cases of polyplex micelles from the block catiomers, PEG-*b*-P[Asp(DET)] polyplex micelles showed much better transfection efficiencies than PEG-*b*-P[Asp(DPT)] polyplex micelles (Fig. 2B), as was the case with the polyplexes from the corresponding homopolymers. With an increase in *N*/*P* ratio, each polyplex micelle showed an increase in transfection activity. Regarding cytotoxicity (Fig. 3), the PEG-*b*-P[Asp(DET)] polyplex micelles always displayed lower cytotoxicity than the

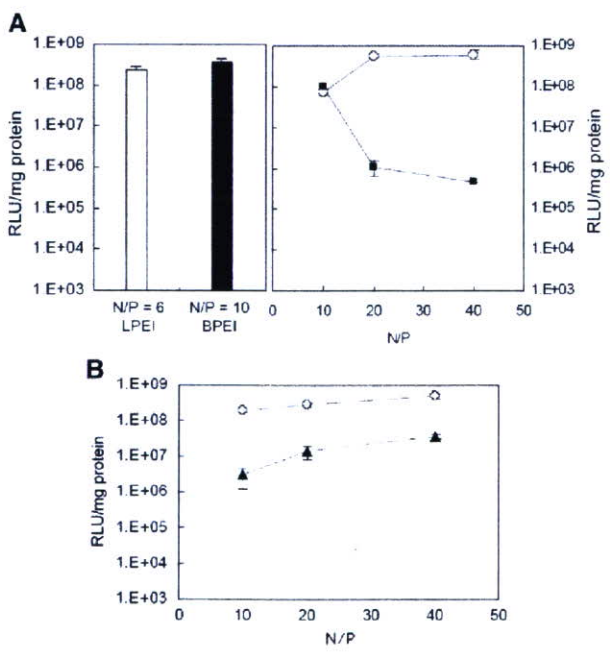

Fig. 2. The transfection of luciferase reporter gene against monolayer cultures of HuH-7. A) Transfection results with L/BPEI polyplexes (*N*/*P*=6 for LPEI according to the manufacturer's recommendation and *N*/*P*=10 for BPEI by optimization), P[Asp(DET)] polyplexes (○) and P[Asp(DPT)] polyplexes (■). B) Transfection results with PEG-*b*-P[Asp(DET)] polyplex micelles (○) and PEG-*b*-P[Asp(DPT)] polyplex micelles (▲).

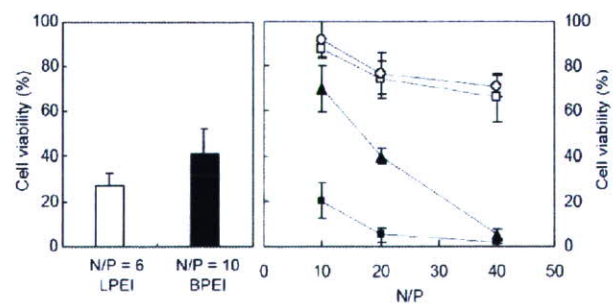

Fig. 3. Cytotoxicity of L/BPEI polyplexes (*N*/*P*=6 for LPEI according to the manufacturer's recommendation and *N*/*P*=10 for BPEI by optimization), P[Asp(DET)] polyplexes (□), P[Asp(DPT)] polyplexes (■), PEG-*b*-P[Asp(DET)] polyplex micelles (○), and PEG-*b*-P[Asp(DPT)] polyplex micelles (▲) toward HuH-7 cells after 48 h incubation.

PEG-*b*-P[Asp(DPT)] polyplex micelles at the same *N*/*P* ratios, and the difference in their cytotoxicity between these polyplex micelles became progressively more significant with increases in the *N*/*P* ratios. The cell viability remained high, and at levels similar between P[Asp(DET)] polyplexes and PEG-*b*-P[Asp (DET)] polyplex micelles, even with increased *N*/*P* ratios. This result suggests that the P[Asp(DET)] structure may have an inherently low cytotoxicity, which was further confirmed by the cytotoxicity assay of free polymers (Supporting Information 1). Notably, PEGylation significantly decreased the cytotoxicity of P[Asp(DPT)], resulting in improved transfection efficacy particularly at higher *N*/*P* ratios. This result clearly indicates that PEGylation is an efficient way to improve the compliance of a polyplex system involving cytotoxic polycations as a component [20]. Nevertheless, the PEGlyation of P[Asp(DET)] did not show any significant effect on cytotoxicity, apparently due to the minimally cytotoxic nature of the P[Asp(DET)] structure.

3.3. Evaluation of characteristic properties of MCTS

Fig. 4 shows the growth of HuH-7 MCTS from the initial diameter of 100 μm. By using Live/Dead assay (live cells: green fluorescence; dead cells: red fluorescence), necrosis of the inner cells of MCTS was observed by a confocal laser scanning microscope (CLSM) when the diameter reached around 400–500 μm (6–8 days after incubation). The necrotic region expanded along with the growth of MCTS. Thus, HuH-7 MCTS clearly took a heterogeneous structure according to the distance from the outer cell layers after they grew beyond the diffusion limit of oxygen and nutrition. Such a growth property represents a good in vitro model for the heterogeneity of solid tumors as a result of the inefficient vascular function [21,22].

3.4. Transfection efficiencies and cytotoxicity of polyplexes and polyplex micelles against MCTS

The gene expression of fluorescent protein *Venus* at defined time periods after transfection with the polyplexes or polyplex micelles was observed by CLSM as shown in Fig. 5. The spheroid diameter at the time of transfection was adjusted to 100 μm to ensure the long-term observation of the transfected gene expression within the optically observable depth range by CLSM. Under this condition, gene expression continued for over 10 days after the transfection and in some cases continued for over 1 month (data not shown). Images of the localization of transfected protein *Venus* in MCTS were taken from the upper surface going towards the center of the MCTS by the z-axis at 1–2 μm intervals of optical slices. Fig. 5A shows typical images of transfected *Venus* in MCTS at different *z*-axes (different distances from the spheroid surface) at 8 days after transfection with PEG-*b*-P[Asp(DET)] polyplex micelles (*N*/*P*=40). The images clearly showed that *Venus* was expressed even at the inner region of MCTS where necrosis was considered to be developed at the corresponding size (Fig. 4).

All the MCTS structures were destroyed after transfection with LPEI or BPEI polyplexes due to their toxicity even at low

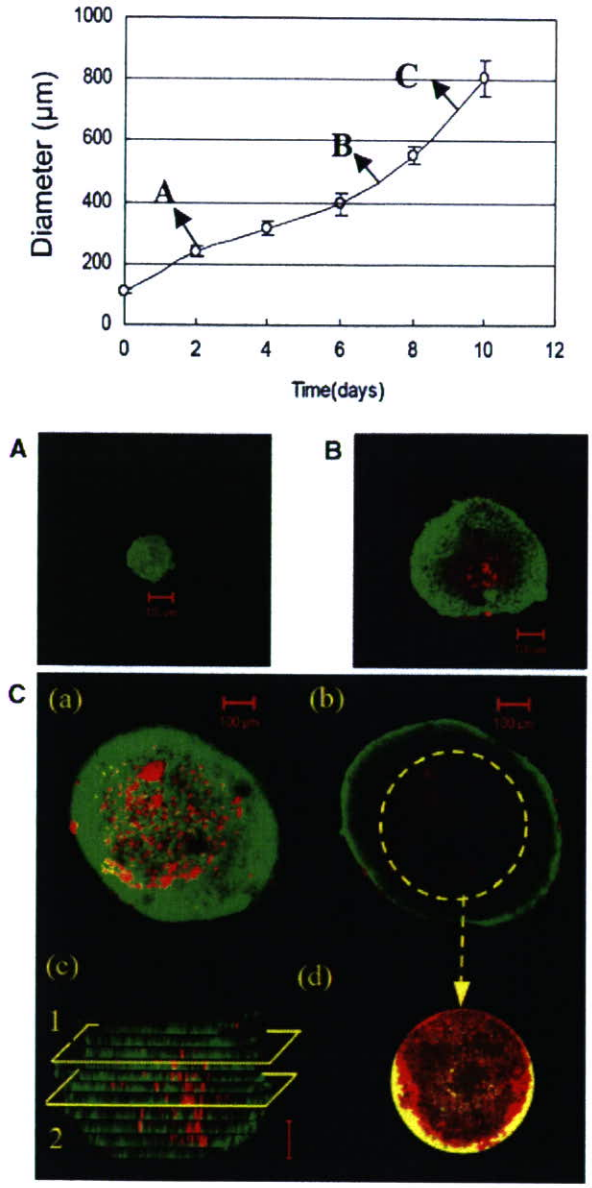

Fig. 4. Growth curve of HuH-7 spheroids and Live/Dead assay of spheroid at each time point of incubation (initial diameter is ca 100 μm. Optical slice at the middle of spheroid. Bar=100 μm. Green and red fluorescence from live and dead cells, respectively). A) 2 days after the formation of MCTS. B) 7 days after the formation of MCTS. C) 9 days after the formation of MCTS. In C, (a) optical slice of spheroid at position 1 of (c); (b) optical slice of spheroid at position 2 of (c); (c) side view of spheroid*; (d) retaken image of region of interest (ROI)**. (*This image was constructed by piling up side views. **This image was taken by stimulating the radiation of ROI by the amplification of laser.)

N/*P* ratios, and thus no systematic data on the spheroid transfection were obtained. P[Asp(DPT)] polyplexes also induced the destruction of MCTS in the whole range of *N*/*P* ratios tested in this study (*N*/*P*=10, 20, and 40). By contrast, P[Asp(DET)] polyplexes showed successful transfection without destruction of the MCTS structure at *N*/*P* ratios of 10 and 20, as seen in Fig. 5B, highlighting the lower cytotoxicity of P[Asp(DET)] compared with P[Asp(DPT)], LPEI, and BPEI. Here,

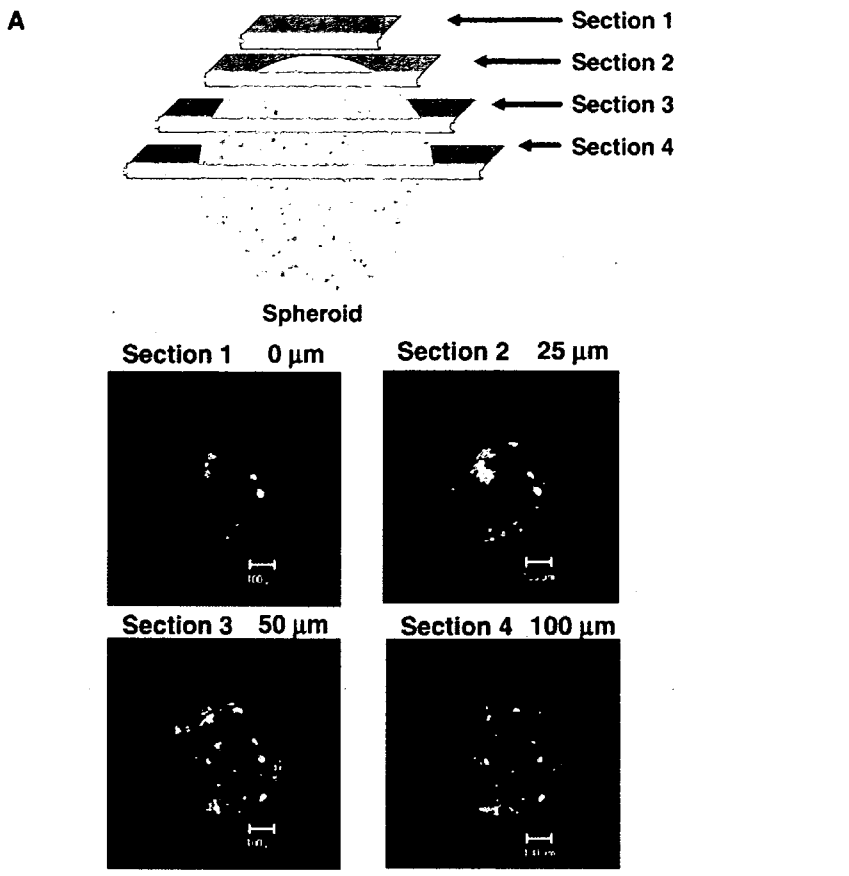
A
Section 1
Section 2
Section 3
Section 4
Spheroid
Section 1 0 μm
Section 2 25 μm
Section 3 50 μm
Section 4 100 μm

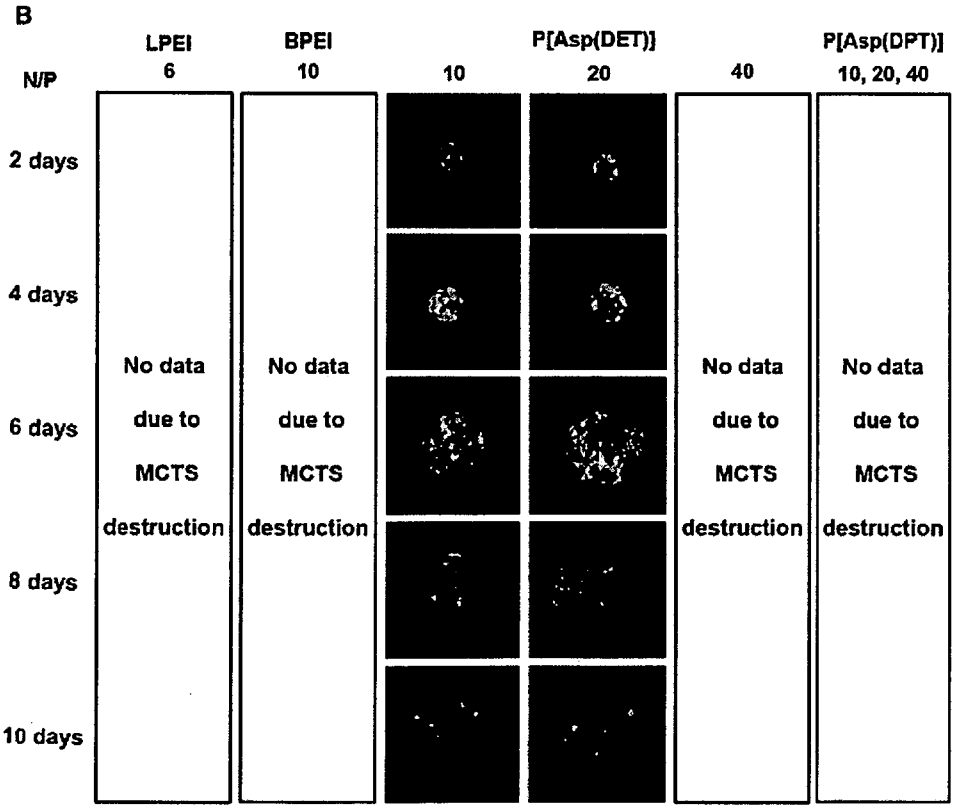
B
LPEI
BPEI
P[Asp(DET)]
P[Asp(DPT)]
N/P
6
10
10
20
40
10, 20, 40
2 days
4 days
6 days
8 days
10 days
No data due to MCTS destruction
No data due to MCTS destruction
No data due to MCTS destruction
No data due to MCTS destruction

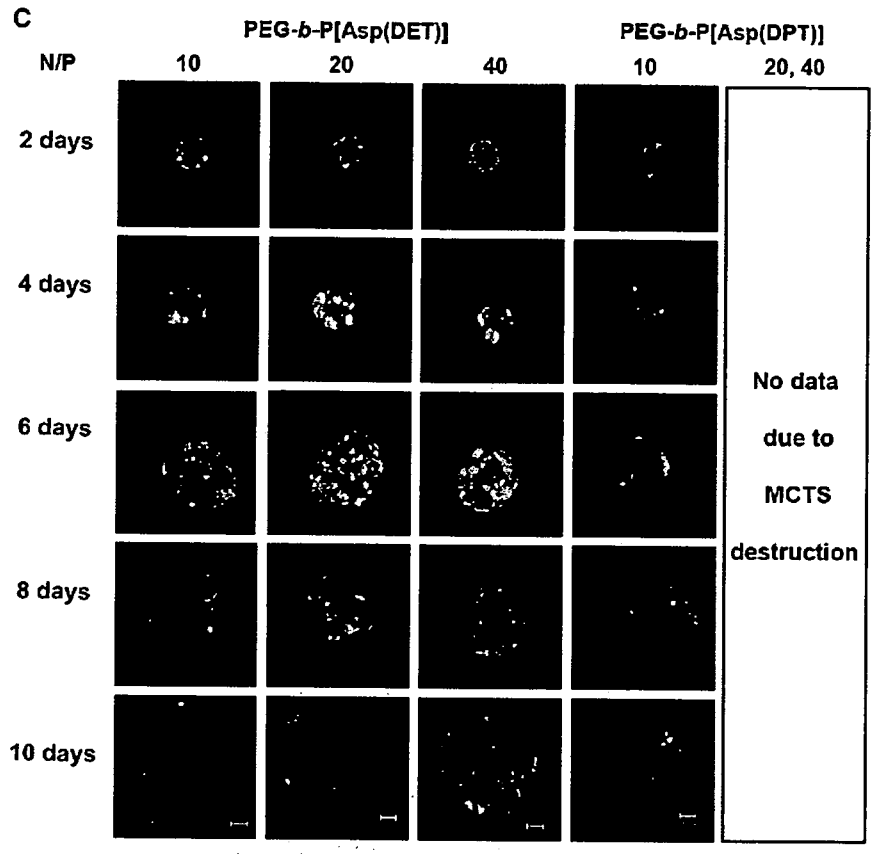

Fig. 5. Expression of marker protein *Venus* in HuH-7 spheroids (initial diameter is ca 100 μm. Bar = 100 μm). A) Localization of transfected *Venus* by PEG-*b*-P[Asp(DET)] polyplex micelles according to the distance from the surface of the spheroid. (The images were the optical slices taken from the upper surface toward the center of the MCTS by the *z*-axis at 0, 25, 50, and 100 μm). B) Optical slices at the middle of spheroids with transfected protein *Venus* by P[Asp(DET)] and P[Asp(DPT)] polyplexes. (Results were not obtained due to the destruction of spheroids after transfection in the cases of *N/P* = 4, 6, 8, 10 for LPEI, *N/P* = 10, 20, 40 for BPEI, *N/P* = 40 for P[Asp(DET)], *N/P* = 10, 20, 40 for P[Asp(DPT)]). C) Optical slices at the middle of spheroids with transfected protein *Venus* by PEG-*b*-P[Asp(DET)] and PEG-*b*-P[Asp(DPT)] polyplex micelles. (Results were not obtained due to the destruction of spheroids after transfection in the cases of *N/P* = 20, 40 for PEG-*b*-P[Asp(DPT)].)

the MCTS images at the middle section by the *z*-axis are shown for each day period. However, even P[Asp(DET)] polyplexes showed the destruction of spheroid structures by increasing the *N/P* ratio to 40.

Overall, PEG-*b*-P[Asp(DET) polyplex micelles showed better transfection activity than PEG-*b*-P[Asp(DPT)] polyplex micelles in MCTS, in agreement with the results of monolayer culture (Fig. 2B). PEG-*b*-P[Asp(DET)] polyplex micelles showed successful activity of the transfection without destruction of MCTS across the range of *N/P* ratios tested in this study (*N/P* = 10, 20, and 40) (Fig. 5C). Worth mentioning is that PEG-*b*-P[Asp(DET)] polyplex micelles did not induce the destruction of spheroids even at *N/P* = 40, where the MCTS structures were destroyed by the transfection with P[Asp(DET)] polyplexes (Fig. 5B) at that *N/P* ratio. Such reduction of cytotoxicity by PEGylation of polycations were not detected by the conventional monolayer culture study (Fig. 3, Supporting Information 1), highlighting high sensitivity of MCTS against polyplex-induced cytotoxicity. While the transfection efficiency of P[Asp(DPT)] was not obtained due to the destruction of MCTS after the transfection, the effect of PEGylation on reducing toxicity was remarkable in this case. Eventually, PEG-*b*-P[Asp(DPT)] polyplex micelles showed appreciable transfection efficiency at the *N/P* ratio of 10.

3.5. Time-dependent gene expression in MCTS

The total fluorescence intensity by *Venus* expression in MCTS was calculated by integrating the intensity image of each optical slice taken from the upper surface going towards the center of the MCTS by the *z*-axis at 1–2 μm intervals (Fig. 5A) using Imaris® software (Fig. 6A). The gene expression by the P[Asp(DET)] polyplexes (*N/P* = 10 and 20) and PEG-*b*-P[Asp(DET)] polyplex micelles (*N/P* = 10, 20, and 40), which showed successful transfection to MCTS, was quantified in this manner at each day period, and the results are shown in Fig. 6B. For both the polyplexes and polyplex micelles, increased the *N/P* ratios led to increased total intensities. Moreover P[Asp(DET)] polyplexes apparently had higher total intensities than PEG-*b*-P[Asp(DET)] polyplex micelles. The total intensity peaked at 6 days after transfection for all the polyplexes and polyplex micelles. It should be noted that such prolonged gene

expression is difficult to detect by the conventional monolayer culture study, because the monolayer cultured cells become confluent until 4 days, beyond which cell viability decreases remarkably. We also evaluated the relative intensity (=total intensity/volume of spheroid) of the expressed *Venus* in the spheroids transfected with the polyplexes or polyplex micelles (Fig. 6C) to normalize the differences in the growth rate and eventually the volume of each spheroid. Although the relative intensity of P[Asp(DET)] polyplexes decreased continuously with time, PEG-*b*-P[Asp(DET)] polyplex micelles with *N/P* ratios of 20 and 40 showed increased relative intensities until 4 days after transfection.

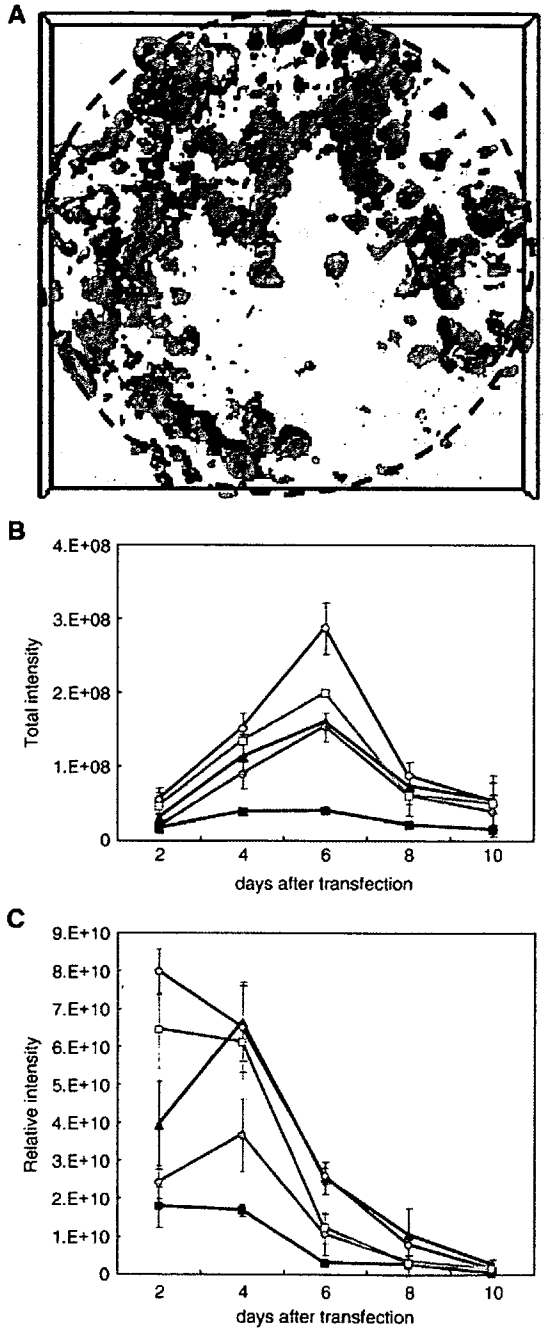

Fig. 6. Quantitative results of transfected fluorescent protein *Venus* in MCTS. A) Piled up images of transfected protein *Venus* from each slice by Imaris® (Carl Zeiss). B) Day-course of the change in total intensity by transfection with P[Asp (DET)] polyplexes (□; *N/P*=10, ○; *N/P*=20) and PEG-*b*-P[Asp(DET)] polyplex micelles (■; *N/P*=10, ●; *N/P*=20, ▲; *N/P*=40). C) Relative intensity (=total intensity/volume of spheroid) of fluorescence from transfected protein *Venus* with P [Asp(DET)] polyplexes (□; *N/P*=10, □; *N/P*=20) and PEG-*b*-P[Asp(DET)] polyplex micelles (■; *N/P*=10, ●; *N/P*=20, ▲; *N/P*=40).

3.6. DOPS-induced destabilization of P[Asp(DET)] polyplex and PEG-b-P[Asp(DET)] micelle

The differences in the time-dependency of the gene expression evaluated from the relative fluorescent intensity between P[Asp (DET)] polyplexes and PEG-*b*-P[Asp(DET)] micelles in Fig. 6C may reflect the differences in their behaviors after the internalization into the cell, because the transfection medium was replaced with fresh medium without polyplexes or micelles after 24 h. We therefore hypothesized that PEG-*b*-P[Asp(DET)] micelles may have greater stability or tolerability against pDNA unpacking, which is presumably induced through the exchange reaction with anionic components in the intracellular compartments, than P[Asp (DET)] polyplexes, thereby showing delayed gene expression. Thus, we evaluated the stability of the polyplex and polyplex micelle in the presence of anionic lipids (DOPS) as natural anionic compounds. It is known that such anionic lipids including phosphatidylserine exist appreciably in the intracellular compartments. As shown in Fig. 7, P[Asp(DET)] polyplexes (*N/P*=20) released pDNA at the [carboxyl groups in DOPS]/[phosphate groups in pDNA] (A/P) ratio of 12, whereas PEG-*b*-P[Asp(DET)] micelles (*N/P*=20) showed no pDNA release even at the highest *A/P* ratio (~17). Thus, PEG-*b*-P[Asp(DET)] micelles were judged to have higher tolerability against DOPS-induced destabilization than P[Asp(DET)] polyplexes.

4. Discussion

In this study, we prepared sets of cationic poly(*N*-substituted asparagine) homopolymers and PEG-*b*-poly(*N*-substituted asparagine) copolymers having the *N*-(2-aminoethyl)-2-aminoethyl group (P[Asp(DET)]) or *N*-(3-aminopropyl)-3-aminopropyl group (P[Asp(DPT)]) in the side chain (Scheme 1) to form polyplex-type non-viral gene vectors. To study the effects of the chemical structures of polycations and the effects of PEGylation of polycations on the properties as non-viral vectors, we carried out gene transfection to HuH-7 cells in the forms of monolayer culture and MCTS.

The in vitro evaluation of non-viral gene vectors relies mostly on the transfection study against monolayer cultured cells. However, there appear to be significant discrepancies between the environments of monolayer culture and in vivo tissues. One of these discrepancies is the short observable terms of the conventional monolayer cultures, which might prevent the study of the time-dependent properties of the gene expression of non-viral vectors. Especially for the polymeric gene delivery systems (polyplexes), in which pDNA is substantially condensed by

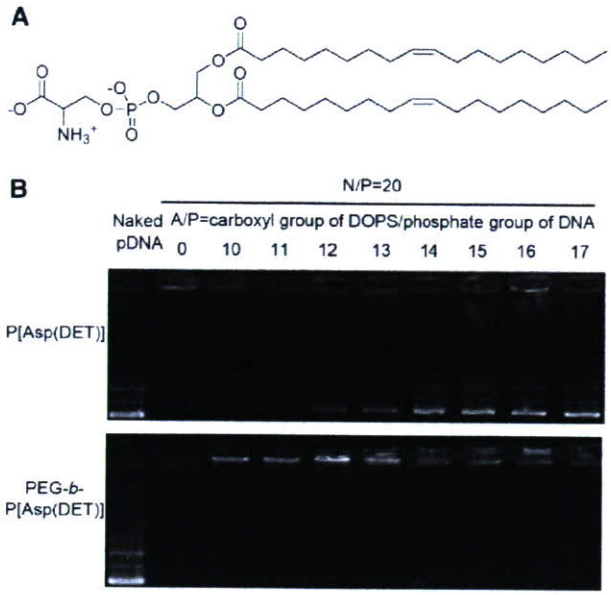

Fig. 7. Electrophoresis of P[Asp(DET)] polyplex and PEG-*b*-P[Asp(DET)] polyplex micelle. A) Chemical structure of anionic lipid (DOPS). B) Electrophoresis of P[Asp(DET)] polyplex and PEG-*b*-P[Asp(DET)] polyplex micelle solutions prepared at the *N*/*P* ratio of 20 after mixing with anionic lipid, DOPS at different *A*/*P* ratios.

cationic polymers and in some cases protected by biocompatible polymers to improve stability in biological media [9–12], prolonged evaluation of the gene expression might be necessary because it may take time for the decondensation and the release (the unpacking process) of pDNA from the polyplexes. Another important discrepancy between in vitro conventional monolayer cultures and in vivo tissues is the three-dimensional environments (e.g., cell–cell and cell–ECM interactions) for the cells. Thus, the three-dimensional features of in vivo tissues should be considered for in vitro evaluation of gene transfection. In this regard, three-dimensional multicellular spheroids (MCTS) might be a promising in vitro model for the evaluation of non-viral vectors worked under in vivo conditions.

In the transfection study using MCTS models, a long-term life span of MCTS might allow the prolonged evaluation of gene expression by non-viral vectors. Indeed, the spheroids transfected with the polyplexes showed the gene expression of fluorescent protein for over 10 days (Figs. 5 and 6). We also found that the small spheroids with diameters of ca 100 μm were more sensitive against the polyplex-induced cytotoxicity than monolayer cultured cells, while relatively large (ca 700 nm) MCTS did not show such high sensitivity to polyplex-induced toxicity (data not shown). It appears that the small spheroids may have a relatively weak structure due to their immature development of cell–cell and cell–ECM interactions. In contrast, the large spheroids have a heterogeneous structure consisting of outer layers of viable cells and a solid core of necrotic or hypoxic cells (Fig. 4C), resembling a monolayer cell culture where the cells adhere to the hard substrate. Such morphological differences between small and large spheroids may account for their different sensitivities against polyplex-induced cytotoxicity.

Among the evaluated polyplexes from the cationic homopolymers, P[Asp(DET)] polyplexes showed the most efficient transfection efficiency with the least cytotoxicity against monolayer cultured cells (Figs. 2 and 3). The efficient transfection by P[Asp(DET)] may be explained by their buffering capacity (Fig. 1A), which may facilitate the cytoplasmic delivery of the polyplexes through destabilization of the endosomal membrane by an increased ion osmotic pressure (proton sponge effect) [2]. However, P[Asp(DPT)] polyplexes at $N/P=10$ also showed an appreciably high transfection activity (Fig. 2A) regardless of the lack of proton buffering capacity (Fig. 1A), suggesting that the proton sponge effect may not fully explain the efficient gene transfection by P[Asp(DPT)] polyplex. Detailed mechanisms involved in the gene transfection process of P[Asp(DET)] and P[Asp(DPT)] polyplexes are under investigation in our laboratory and will be reported elsewhere in the near future. The cytotoxicity of P[Asp(DET)] polyplexes was remarkably low compared with other polyplexes from P[Asp(DPT)] or L/BPEI (Fig. 3). Also, the transfection study using MCTS models revealed that P[Asp(DET)] polyplexes at $N/P=10$ and 20 showed successful transfection with maintaining the MCTS structures, while the destruction of MCTS occurred by challenging L/BPEI and P[Asp(DPT)] polyplexes (Fig. 5B). The destruction of MCTS by the polyplexes (Fig. 5B) is in line with the cytotoxicity of the polyplexes against the monolayer cultured cells (Fig. 3), indicating the minimally cytotoxic nature of P[Asp(DET)] polyplexes. The unique molecular feature of a franking ethylenediamine unit, including a specific *gauche*-conformation of the mono-protonated form preferential at the physiological state, may have a role in this appreciably high biocompatibility of P[Asp(DET)] polyplexes. This hypothesis remains to be clarified yet.

PEGylation of polycations apparently improved the biocompatibility of polyplexes, as indicated by the stability of the MCTS structure after transfection. The PEG-*b*-P[Asp(DPT)] polyplex micelles at $N/P=10$ did not cause the destruction of the MCTS (Fig. 5C), whereas the destruction occurred through the transfection with P[Asp(DPT)] polyplexes at the same *N*/*P* ratio (Fig. 5B). Likewise, the PEG-*b*-P[Asp(DET)] polyplex micelles at $N/P=40$ showed no MCTS destruction, while the destruction of MCTS was observed in the transfection with the P[Asp(DET)] polyplexes at the same *N*/*P* ratio. Note that such a difference in biocompatibility between PEG-*b*-P[Asp(DET)] polyplex micelles and P[Asp(DET)] polyplexes could not be detected by the cytotoxicity study using the monolayer cultured cells, but was detected using the MCTS models. This result suggests that MCTS models are more sensitive than monolayer cultured cells to polyplex-induced toxicity, allowing them to detect the improved biocompatibility of the polyplex system through the PEGylation of polycations. Besides its positive effect of improving the cytotoxicity of the polyplexes, PEGylation of the polyplex changed the time-dependent profiles of the transfected gene expression. As seen in Fig. 6C, the relative intensity of the transfected fluorescent protein (i.e., *Venus*) in MCTS, which is defined as the total intensity divided by the volume of spheroids, followed significantly different time courses between P[Asp(DET)] polyplexes and PEG-*b*-P[Asp(DET)] polyplex micelles: the latter with relatively high *N*/*P* ratios, such as 20 and 40, had peak relative intensities at 4 days after transfection, while the former exhibited a continuous decrease in the relative

intensities with time (Fig. 6C). These results suggest that the polyplex micelles from PEG-*b*-polycation copolymers may be capable of delaying gene expression compared with polyplexes from cationic homopolymers. This is consistent with our previous report that in vivo gene expression of polyplex micelles in the liver revealed a delayed onset, and was observed 5 days after intravenous injection [13]. We hypothesized that such delayed gene expression from the polyplex micelles might be due to their higher stability or their delayed unpacking of pDNA in intracellular compartments. This may be supported from the increased tolerability of PEG-*b*-P[Asp(DET)] polyplex micelles compared to P[Asp(DET)] polyplexes against the pDNA exchange reaction with an anionic lipid, DOPS (Fig. 7). It is also consistent with our previous report that PEG-*b*-poly(L-lysine) polyplex micelles showed higher stability than poly(L-lysine) polyplexes in the thermal melting study of DNA [8]. The decrease in the local permittivity of the polyplex core, surrounded by PEG palisades and/or a steric protection of the polyplex core by PEG palisades, may contribute to the stabilization of polyplex micelles against the exchange reaction with anionic components in intracellular environments. It is worth noting that the time-dependency of gene expression differs between polyplex systems, which was clearly investigated through the prolonged observation of transfected cells in the form of spheroids.

In conclusion, we used MCTS models to study the effects of chemical structures and PEGylation of cationic poly(*N*-substituted asparagine) polyplexes on gene transfection, particularly focusing on both polyplex toxicity and the duration of gene expression. Through this evaluation, the feasible properties, i.e., biocompatibility and prolonged gene expression, of PEG-*b*-P[Asp(DET)] micelles were clarified, facilitating their utility for in vivo gene transfection as recently demonstrated in a rabbit carotid artery model [15]. Also, this study underscores the usefulness of MCTS models in screening non-viral vectors in conditions mimicking in vivo environments.

Acknowledgement

We are grateful to Mr. S. Fukushima and Mr. S. Asano for polymer synthesis. This work was supported by the Core Research for Evolutional Science and Technology (CREST), Japan Science and Technology Agency (JST), and the Health and Labor Sciences Research Grants in Research on Advanced Medical Technology in Nanomedicine Area from the Ministry of Health, Labor and Welfare (MHLW), Japan.

Appendix A. Supplementary data

Supplementary data associated with this article can be found, in the online version, at doi:10.1016/j.jconrel.2007.05.012.

References

[1] G.Y. Wu, C.H. Wu, Receptor-mediated in vitro gene transformation by a soluble DNA carrier system, J. Biol. Chem. 262 (1987) 4429–4432.
[2] O. Boussif, F. Lezoualc'h, M.A. Zanta, M.D. Mergny, D. Scherman, B. Demeneix, J.P. Behr, A versatile vector for gene and oligonucleotide transfer into cells in culture and in vivo: Polyethyleneimine, Proc. Natl. Acad. Sci. U. S. A. 92 (1995) 7297–7301.
[3] D.W. Pack, A. Hoffman, S. Pun, P.S. Stayton, Design and development of polymers for gene delivery, Nat. Rev. Drug. Discov. 4 (2005) 581–593.
[4] A.V. Kabanov, I.V. Astafieva, I.V. Maksimova, E.M. Lukanidin, G.P. Georgiev, V.A. Kabanov, Efficient transformation of mammalian cells using DNA interpolyelectrolyte complexes with carbon chain polycations, Bioconjug. Chem. 4 (1993) 448–454.
[5] M. Harada-Shiba, K. Yamauchi, A. Harada, I. Takamisawa, K. Shimokado, K. Kataoka, Polyion complex micelles as vectors in gene therapy — pharmacokinetics and in vivo gene transfer, Gene Ther. 9 (2002) 407–414.
[6] M. Ogris, E. Wagner, Targeting tumors with non-viral gene delivery systems, Drug Discov. Today 7 (2002) 479–485.
[7] K. Kataoka, G.S. Kwon, M. Yokoyama, T. Okano, Y. Sakurai, Block copolymer micelles as vehicles for drug delivery, J. Control. Release 24 (1993) 119–132.
[8] S. Katayose, K. Kataoka, Water-soluble polyion complex associates of DNA and poly(ethylene glycol)-poly(l-lysine) block copolymer, Bioconjug. Chem. 8 (1997) 702–707.
[9] M. Ogris, S. Brunner, S. Schüller, S. Kircheis, E. Wagner, PEGylated DNA/transferrin-PEI complexes: reduced interaction with blood components, extended circulation in blood and potential for systemic gene delivery, Gene Ther. 6 (1999) 595–605.
[10] T. Merdan, K. Kunath, H. Petersen, U. Bakowsky, K.H. Voigt, J. Kopecek, T. Kissel, PEGylation of poly(ethylene imine) affects stability of complexes with plasmid DNA under in vivo conditions in a dose-dependent manner after intravenous injection in to mice, Bioconjug. Chem. 16 (2005) 785–792.
[11] K. Itaka, A. Harada, K. Nakamura, H. Kawaguchi, K. Kataoka, Evaluation by fluorescence resonance energy transfer of the stability of nonviral gene delivery vectors under physiological conditions, Biomacromolecules 3 (2002) 841–845.
[12] K. Itaka, K. Yamauchi, A. Harada, K. Nakamura, H. Kawaguchi, K. Kataoka, Polyion complex micelles from plasmid DNA and poly(ethylene glycol)-poly (l-lysine) block copolymers as serum-tolerable polyplex system: physicochemical properties of micelles relevant to gene transfection efficiency, Biomaterials 24 (2003) 4495–4506.
[13] K. Miyata, Y. Kakizawa, N. Nishiyama, Y. Yamasaki, T. Watanabe, M. Kohara, K. Kataoka, Freeze-dried formulations for in vivo gene delivery of PEGylated polyplex micelles with disulfide crosslinked cores to the liver, J. Control. Release 109 (2005) 15–23.
[14] N. Kanayama, S. Fukushima, N. Nishiyama, K. Itaka, W.D. Jang, K. Miyata, Y. Yamasaki, U.I. Chung, K. Kataoka, A PEG-based biocompatible block catiomer with high buffering capacity for the construction of polyplex micelles showing efficient gene transfer toward primary cells, Chem. Med. Chem. 1 (2006) 439–444.
[15] D. Akagi, M. Oba, H. Koyama, N. Nishiyama, S. Fukushima, T. Miyata, H. Nagawa, K. Kataoka, Biocompatible micellar nanovectors achieve efficient gene transfer to vascular lesions without cytotoxicity and thrombus formation. Gene Therapy, in press.
[16] R.M. Sutherland, Cell and environment interactions in tumor microregions: the multicell spheroid model, Science 240 (1988) 177–184.
[17] H.R. Mellor, L.A. Davies, H. Caspar, C.R. Pringle, S.C. Hyde, D.R. Gill, R. Callaghan, Optimising non-viral gene delivery in a tumour spheroid model, J. Gene Med. 8 (2006) 1160–1170.
[18] H. Niwa, K. Yamamura, J. Miyazaki, Efficient selection for high-expression transfectants with a novel eukaryotic vector, Gene 108 (1991) 193–199.
[19] T. Nagai, K. Ibata, E.S. Park, M. Kubota, K. Mikoshiba, A. Miyawaki, A variant of yellow fluorescent protein with fast and efficient mutation for cell-biological application, Nat. Biotechnol. 20 (2002) 87–90.
[20] G.P. Tang, J.M. Zeng, S.J. Gao, Y.X. Ma, L. Shi, Y. Li, H.P. Too, S. Wang, Polyethylene glycol modified polyethylenimine for improved CNS gene transfer, Biomaterials 24 (2003) 2351–2362.
[21] M. Haji-Karim, J. Carlsson, Proliferation and viability in cellular spheroids of human origin, Cancer Res. 38 (1978) 1457–1464.
[22] L.A. Kunz-Schughart, Multicellular tumor spheroids; intermediates between monolayer culture and in vivo tumor, Cell Biol. Int. 23 (1999) 157–161.

VOLUME 121 NO. 3, 28 AUGUST 2007 ISSN: 0168-3659

journal of
controlled
release

OFFICIAL JOURNAL OF THE CONTROLLED RELEASE SOCIETY
AND THE JAPANESE SOCIETY OF DRUG DELIVERY SYSTEM

Available online at www.sciencedirect.com
ScienceDirect
Journal of Controlled Release 121 (2007) 146–155
journal of controlled release
www.elsevier.com/locate/jconrel

Optimization of (1,2-diamino-cyclohexane)platinum(II)-loaded polymeric micelles directed to improved tumor targeting and enhanced antitumor activity

Horacio Cabral [a], Nobuhiro Nishiyama [b], Kazunori Kataoka [a,b,c,*]

[a] Department of Materials Engineering, Graduate School of Engineering, The University of Tokyo, 7-3-1 Hongo, Bunkyo-ku, Tokyo 113-8656, Japan
[b] Center for Disease Biology and Integrative Medicine, Graduate School of Medicine, The University of Tokyo, 7-3-1 Hongo, Bunkyo-ku, Tokyo 113-0033, Japan
[c] Center for NanoBio Integration, The University of Tokyo, 7-3-1 Hongo, Bunkyo-ku, Tokyo, 113-8656, Japan

Received 19 March 2007; accepted 21 May 2007
Available online 29 May 2007

Abstract

Polymeric micelles are promising nanocarriers, which might enhance the efficacy of antitumor drugs. Herein, polymeric micelles incorporating dichloro(1,2-diamino-cyclohexane)platinum(II) (DACHPt), the oxaliplatin parent complex, were prepared through the polymer-metal complex formation of DACHPt with poly(ethylene glycol)-*b*-poly(glutamic acid) [PEG-*b*-P(Glu)] block copolymer having different lengths of the poly (glutamic acid) block [p(Glu): 20, 40, and 70 U]. The resulting micelles were studied with the aim of optimizing the system's biological performance. DACHPt-loaded micelles (DACHPt/m) were approximately 40 nm in diameter and had a narrow size distribution. *In vivo* biodistribution and antitumor activity experiments (CDF_1 mice bearing the murine colon adenocarcinoma C-26 inoculated subcutaneously) showed 20-fold greater accumulation of DACHPt/m at the tumor site than free oxaliplatin to achieve substantially higher antitumor efficacy. Moreover, the micelles prepared from PEG-*b*-P(Glu) with 20 U of P(Glu) exhibited the lowest non-specific accumulation in the liver and spleen to critically reduce non-specific accumulation, resulting in higher specificity to solid tumors. The antitumor effect of DACHPt/m was also evaluated on multiple metastases generated from intraperitoneally injected bioluminescent HeLa (HeLa-Luc) cells. The *in vivo* bioluminescent data indicated that DACHPt/m decreased the signal 10-to 50-fold compared to the control indicating a very strong antitumor activity. These results suggest that DACHPt/m could be an outstanding drug delivery system for oxaliplatin in the treatment of solid tumors.

Keywords: Polymeric micelles; DACHPt; Oxaliplatin; Biodistribution; Antitumor activity

1. Introduction

Oxaliplatin, oxalato(trans-*l*-1,2-diaminocyclohexane)platinum(II), is a third-generation platinum drug approved by the United States Food and Drug Administration in 2004 for the first-line treatment of advanced colorectal cancer in combination with 5-fluorouracil/folinic acid (5-FU/LV) [1]. The incorporation of oxaliplatin into the colorectal cancer program represents a major improvement in the treatment of the disease. The synergistic effects between oxaliplatin and 5-FU/LV significantly increased the response rates, improved the time-sensitive response parameters, and contributed to the removal of heretofore unresectable hepatic metastases, thereby changing the natural history of the malignancy. Nevertheless, oxaliplatin distributes rapidly to the whole body and, even though it shows better tolerability relative to other platinum drugs, cumulative peripheral distal neurotoxicity and acute dysesthesias restrain the range of working doses [2,3]. Consequently, enormous effort has been dedicated to develop drug delivery systems that increase the blood residence time of oxaliplatin and other platinum drugs, and target those drugs to solid tumors by taking advantage of the enhanced permeability and retention (EPR) effect [4]. Liposomes and macromolecular carriers (water soluble polymer–drug conjugates) have been the first attempts

* Corresponding author. Department of Materials Engineering, Graduate School of Engineering, The University of Tokyo, 7-3-1 Hongo, Bunkyo-ku, Tokyo 113-8656, Japan. Tel.: +81 3 5841 7138; fax: +81 3 5841 7139.
E-mail address: kataoka@bmw.t.u-tokyo.ac.jp (K. Kataoka).

0168-3659/$ - see front matter © 2007 Elsevier B.V. All rights reserved.
doi:10.1016/j.jconrel.2007.05.024

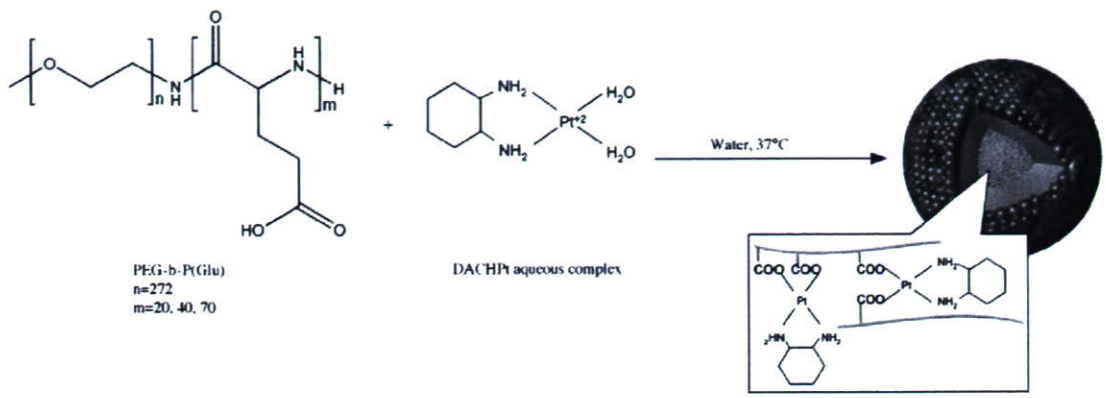

Fig. 1. Formation of DACHPt-loaded micelle (DACHPt/m).

to be considered [5–11]. However, successful formulations have not been developed yet due to unfavorable properties of platinum drugs. For example, the low water solubility of platinum drugs limits their loading efficacy into liposomal formulations (only 1 to 7% of drug loading). Moreover, liposomes incorporating the drug in the lipid bilayer showed rapid leakage of the drugs during storage and in the bloodstream [6]. In the case of macromolecular-drug formulations at high substitution ratios, they show reduced solubility due to the enlarged cohesive forces and to the cross-linking formation between polymer chains [8].

A novel approach to the design of nanocarriers for platinum drugs has been utilizing polymeric micelles [12–15]. Polymeric micelles present unique advantages over other types of drug-carrier systems: (i) prolonged blood circulation due to the efficient stealthy behavior of the dense shell of poly(ethylene glycol) (PEG), which hinders the adsorption of plasma proteins on the surface of the nanostructure and avoids recognition by the reticuloendothelial system (RES); (ii) easiness in encapsulating different compounds by modulating the micelle-forming block copolymers; (iii) reduced cumulative toxicity because of the micellar self-dissociation into unimers with molecular weight lower than that of the threshold of glomerular excretion; (iv) simplicity in size control by changing the chemical composition of block copolymers; (v) deeper tumor penetration due to the sub-100 nm size; (vi) facile management of the drug release in a controlled and environment-sensitive manner by modification of the drug-polymer system; and (vii) improved targeting capability by conjugating pilot molecules on the surface of micelles.

The first generation of platinum-drug-loaded micelles was prepared by the metal-complex formation between cis-dichlorodiammineplatinum(II) (cisplatin, CDDP) and poly(ethylene glycol)-*b*-poly(amino acid) block copolymers [16–21]. The exceptional physicochemical and biological properties of the CDDP-loaded micelle indicate them as an outstanding delivery system for CDDP complexes and a phase I clinical trial is being performed in United Kingdom (NC-6004, Nanocarrier, Japan). More recently, new platinum-drug-loaded polymeric micelles incorporating the oxaliplatin active complex were prepared by the complexation of dichloro(1,2-diaminocyclohexane)platinum(II) (DACHPt) with PEG-*b*-P(Glu) [22]. Previous studies demonstrated that the DACHPt-loaded micelle (DACHPt/m) might maintain its micellar structure for approximately 10 days in 10 mM PBS plus 150 mM NaCl, considerably longer than the stability of the CDDP-loaded micelles (ca 50 h) under the same conditions, while the drug was released from the micelle core in a sustained manner. Moreover, DACHPt/m showed remarkably prolonged blood circulation and more than 20-fold greater accumulation in tumor tissue compared to free oxaliplatin. According to these results, DACHPt/m seems to be an exceptionally promising carrier for the active complexes of oxaliplatin.

Herein, the *in vitro* and *in vivo* biological properties of DACHPt/m prepared with poly(ethylene glycol)-*b*-poly(glutamic acid) [PEG-*b*-P(Glu)] were studied with the aim of optimizing the biological performance of the micelle. Thus, PEG-*b*-P(Glu) having different P(Glu) block lengths (20, 40, and 70 U) were synthesized and used for the micelle preparation. DACHPt/m was phisicochemically characterized to determine the size, size distribution, zeta-potential, drug loading, and weight fraction of block copolymer. The *in vivo* behavior of DACHPt/m was assessed by the biodistribution and antitumor activity experiments using CDF_1 mice bearing the murine colon adenocarcinoma 26 (C-26). Although oxaliplatin had shown low efficacy against this tumor model [23], we found that DACHPt/m considerably increased the antitumor activity of the drug, probably by maintaining high drug levels within the tumor for a prolonged period. Furthermore, since chemotherapy is used in patients with metastatic disease and all the established therapies reveal poor efficiency at the late stage of the disease [24], new therapeutic strategies are urgently needed. Moreover, given that the very low prognosis of late-stage cervical carcinoma [25] (5 years after treatment 15% or fewer of women with stage IV cancer survive) is mainly due to metastasis to the abdomen or the lungs, the antitumor activity of DACHPt/m was evaluated against a bioluminescent intraperitoneal metastatic tumor model of cervical cancer.

2. Experimental

2.1. Materials

γ-benzyl L-glutamate was purchased from Sigma Chemical (St. Louis, MO). Bis(trichloromethyl)carbonate (triphosgene) was purchased from Tokyo Kasei Kogyo (Tokyo, Japan). *N,N*-

Table 1
DACHPt-loaded micelles (DACHPt/m) size, zeta-potential and drug loading

Micelle formulation	Size(nm)	Zeta-potential(mV)	Drug loading, [DACHPt]/[Glu]
DACHPt/m 12–20	37	−3	0.317
DACHPt/m 12–40	40	−4	0.323
DACHPt/m 12–70	41	−4	0.288

dimethylformamide (DMF) and 3-(4,5-dimethylthiazol-2-yl)-2,5-diphenyltetrazolium bromide (MTT) were obtained from Wako Pure Chemical (Osaka, Japan). Dichloro(1,2-diammino-cyclohexane)platinum(II) (DACHPt) and $AgNO_3$ were purchased from Aldrich Chemical (Milwaukee, WI). α-methoxy-ω-aminopoly(ethylene glycol) (CH_3O–PEG–NH_2; Mw= 12,000) was purchased from Nippon Oil and Fats (Tokyo, Japan).

2.2. Cell lines and animals

Murine colon adenocarcinoma 26 (C-26) cells were kindly supplied by the National Cancer Center (Tokyo, Japan). C-26 cells were maintained in RPMI 1640 medium (Sigma Chemical) containing 10% fetal bovine serum in a humidified atmosphere containing 5% CO_2 at 37 °C. Bioluminescent HeLa (HeLa-Luc) cells were purchased from Xenogen (Alameda, CA). Luciferase stable-HeLa-Luc cells were maintained in Dulbecco's Modified Eagle Medium (Sigma Chemical Co., Inc.) containing 10% fetal bovine serum in a humidified atmosphere containing 5% CO_2 at 37 °C for no more than two weeks to assure luciferase luminescence stability.

Table 2
Accumulation ratios and area under the curve (AUC) ratios between tumor and normal organs at 48 h after administration of DACHPt-loaded micelles (DACHPt/m)[a] prepared with PEG-*b*-P(Glu) 12–40 and free oxaliplatin

Drug	Accumulation ratio				AUC ratio[b]	
	Tumor/ liver	Tumor/ spleen	Tumor/ kidney	Tumor/ liver	Tumor/ spleen	Tumor/ kidney
DACHPt/m 12–40	1.25	1.26	3.9	1.25	1.53	3.12
Oxaliplatin	0.9	0.18	0.42	1.1	0.32	0.9

[a] Dose: 0.1 mg per mouse on Pt basis.
[b] AUC calculated by trapezoidal rule up to 48 h.

Severe Combined Immunodeficiency (SCID) and CDF_1 mice (female; 18–20 g body weight; 6 weeks old) were purchased from Charles River Japan (Kanagawa, Japan). All animal experiments were carried out in accordance with the Guide for the Care and Use of Laboratory Animals as stated by the NIH. Sterile procedures were followed to assure that SCID mice were disease-free.

2.3. Preparation of PEG-b-P(Glu)

PEG-*b*-P(Glu) block copolymers were synthesized in accordance with the previously described synthetic method

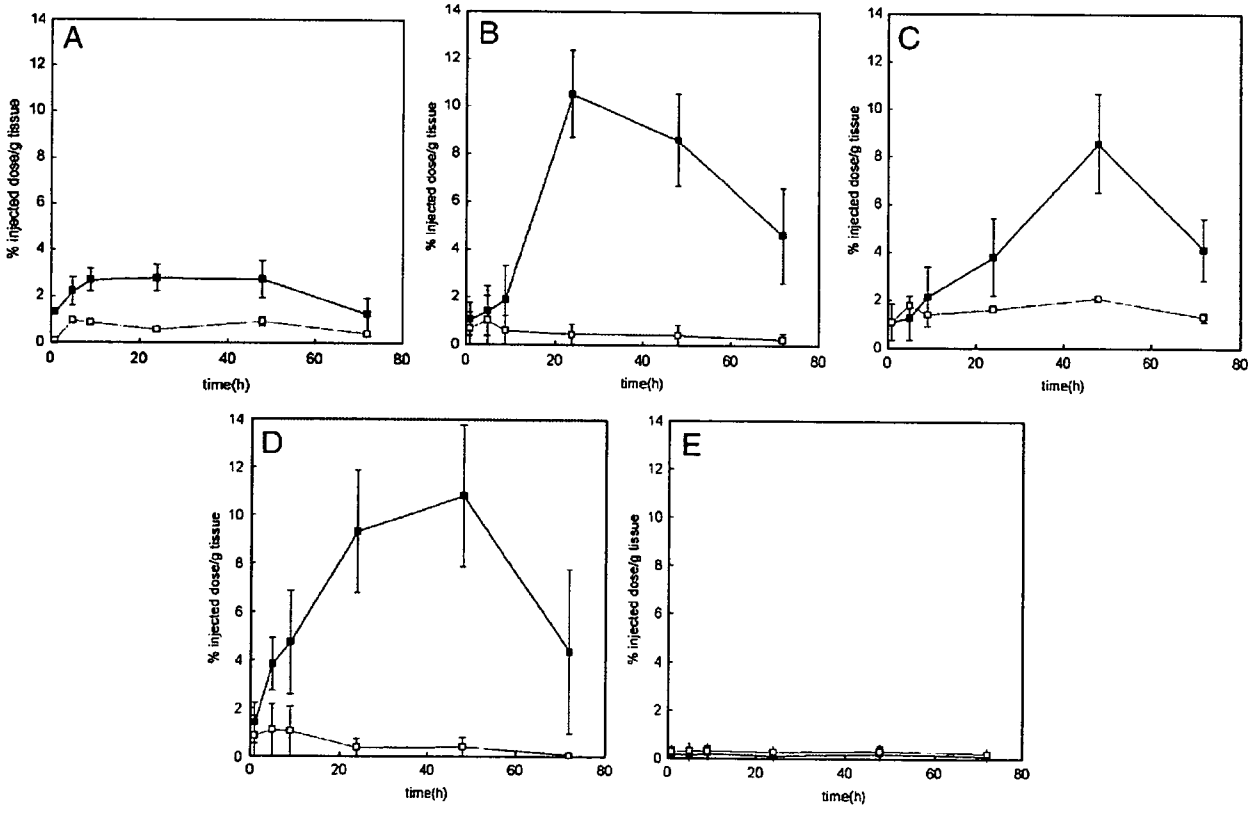

Fig. 2. Biodistribution of oxaliplatin (□) and DACHPt-loaded micelle (DACHPt/m) prepared with PEG-*b*-P(Glu) 12–40 (■): A. Kidney; B. Liver; C. Spleen; D. Tumor; E. Muscle. Data are expressed as averages±S.D.

[20] with a minor modification. Briefly, the *N*-carboxy anhydride of γ-benzyl L-glutamate was synthesized by the Fuchs–Farthing method using triphosgene. Then, *N*-carboxy anhydride of γ-benzyl L-glutamate was polymerized in DMF, initiated by the primary amino group of CH_3O–PEG–NH_2, to obtain PEG-*b*-poly(γ-benzyl L-glutamate) (PEG-*b*-PBLG) block copolymer with different PBLG block lengths (20, 40, and 70 U). The molecular weight distribution of PEG-*b*-PBLG was determined by gel permeation chromatography [column: TSK-gel $G3000_{HHR}$, $G4000_{HHR}$ (Tosoh, Yamaguchi, Japan); eluent: DMF containing 10 mM LiCl; flow rate: 0.8 ml/min; detector: refractive index (RI); temperature: 25 °C]. The polymerization degree of PBLG was verified by comparing the proton ratios of methylene units in PEG (–OCH_2CH_2–: δ=3.7 ppm) and phenyl groups of PBLG (–$CH_2C_6H_5$: δ=7.3 ppm) in ^{1}H-NMR measurement [JEOL EX270 (JEOL, Tokyo, Japan); solvent: DMSO-d_6; temperature: 80 °C]. PEG-*b*-PBLG was deprotected by mixing with 0.5 N NaOH at room temperature to obtain PEG-*b*-P(Glu). Complete deprotection was confirmed by ^{1}H-NMR measurement (solvent: D_2O; temperature: 25 °C). The compositions of PEG-*b*-P(Glu) are abbreviated as PEG-*b*-P(Glu) 12–20, PEG-*b*-P(Glu) 12–40 and PEG-*b*-P(Glu) 12–70 for the different P(Glu) block lengths (20, 40, and 70 U, respectively).

2.4. Preparation of DACHPt-loaded micelles (DACHPt/m)

DACHPt/m were prepared according to a previously described method [22]. Briefly, DACHPt (5 mM) was suspended in distilled water and mixed with silver nitrate ([$AgNO_3$]/[DACHPt]=1) to form an aqueous complex. The solution was kept in the dark at 25 °C for 24 h. AgCl precipitates found after the reaction were eliminated by centrifugation. Afterward, the supernatant was purified by passage through a 0.22 μm filter. Then, PEG-*b*-P(Glu) 12–20, 12–40, or 12–70 ([Glu]=5 mmol/liter) was added to DACHPt aqueous complex solution ([DACHPt]/[Glu]=1.0) and reacted for 120 h to prepare DACHPt/m. The prepared micelles were purified by ultrafiltration [molecular weight cutoff size (MWCO): 100,000]. The size distribution of DACHPt/m was evaluated by the dynamic light scattering (DLS) measurement at 25 °C using a Photal DLS-7000 dynamic laser scattering spectrometer (Otsuka Electronics, Osaka, Japan). The zeta-potential of DACHPt/m was determined using a Zetasizer Nano ZS90 (Malvern Instruments, Worcestershire, United Kingdom). The Pt content of the micelles was determined by an ion coupled plasma-mass spectrometer (4500 ICP-MS; Hewlett Packard, Palo Alto, CA).

2.5. Biodistribution

In order to analyze the fate of oxaliplatin and DACHPt/m *in vivo*, CDF_1 mice (female, n=6) were injected subcutaneously with C-26 cells (1×10^6 cells/ml). Fourteen days later, oxaliplatin or DACHPt/m prepared with PEG-*b*-P(Glu) 12–40 were intravenously injected by the tail vein at a dose of 100 μg/mouse on a platinum basis. Mice were sacrificed after defined time periods (1, 4, 8, 24, 48, and 72 h).

To assess the effect of formulation on the tissue distribution, CDF_1 mice (female, n=6) bearing s.c. C-26 tumors were intravenously administered oxaliplatin or DACHPt/m prepared with PEG-*b*-P(Glu) with different P(Glu) lengths (20, 40, and

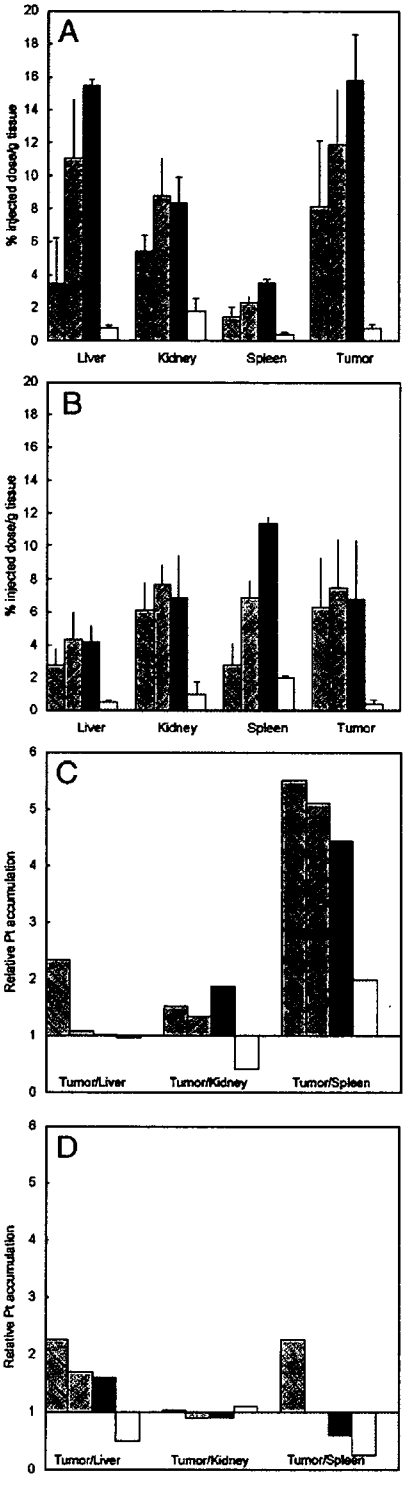

Fig. 3. Biodistribution of DACHPt-loaded micelle (DACHPt/m) prepared with PEG-*b*-P(Glu) 12–20(▨), PEG-*b*-P(Glu) 12–40(▨), PEG-*b*-P(Glu) 12–70(■) and oxaliplatin (□): A. 24 h; B.48 h; C. 24 h tumor/organ ratio; D. 48 h tumor/organ ratio. Data are expressed as averages±S.D.

70 U) at 100 μg/mouse on a platinum basis. Mice were sacrificed at 24 and 48 h post-incubation.

Tumor, liver, kidney, spleen, and muscle were collected. Blood was collected from the inferior vena cava, heparinized and centrifuged to obtain the plasma. Tissue samples were washed in ice-cold saline and weighed after removing excess fluid. All samples were dissolved in HNO_3 and evaporated to dryness. The Pt concentration was measured by ICP-MS after the samples were redissolved in 5 N HCl. The area under the curve (AUC) was calculated by the trapezoidal rule.

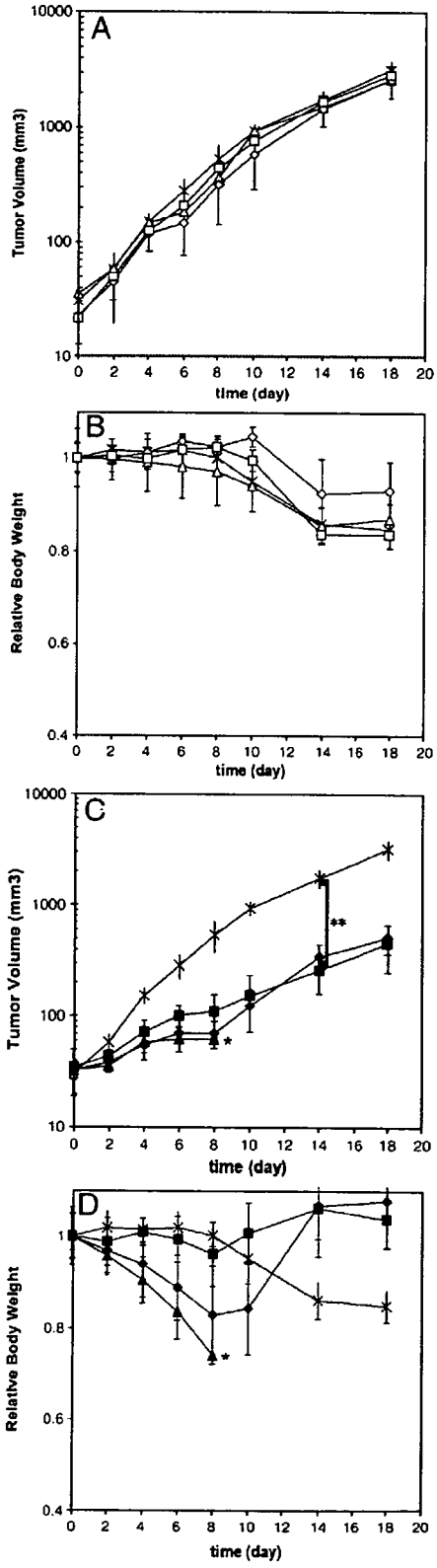

2.6. Antitumor activity assay

CDF_1 mice (female, $n=6$) were inoculated subcutaneously with C-26 cells (1×10^6 cells/ml). Tumors were allowed to grow for 1 week (the size of tumor at this point was approximately 30 mm^3 or 100 mm^3). Subsequently, mice were treated i.v. 4 times at 2-day intervals at doses of 2, 4, 6 and 10 mg/kg of oxaliplatin or 2, 4 and 6 mg/kg (on a platinum base) of DACHPt/m prepared with PEG-*b*-P(Glu) 12–20 or PEG-*b*-P (Glu) 12–40. The antitumor activity was evaluated in terms of tumor size (V), as estimated by the following equation:

$$V = a \times b^2/2$$

where a and b are the major and minor axes of the tumor measured by a caliper, respectively. The body weight was measured simultaneously and was taken as a parameter of systemic toxicity. The statistical analysis of animal data was carried out by the unpaired t-test.

2.7. Antitumor activity in a bioluminescent intraperitoneal metastasis model

SCID mice (female, $n=5$) were inoculated intraperitoneally with Hela-Luc cells (5×10^5 cells/ml). Tumors were allowed to grow for 3 days. Subsequently, mice were treated i.v. 3 times at 2-day intervals at doses of 4 and 6 mg/kg (on a platinum base) of oxaliplatin or DACHPt/m prepared with PEG-b-P(Glu) 12–20. *In vivo* bioluminescent imaging (BLI) was performed with an IVIS Imaging System (Xenogen) comprised of a highly sensitive, cooled CCD camera mounted in a light-tight specimen box. Images and measurements of bioluminescent signals were acquired and analyzed using Living Image software (Xenogen). Ten minutes prior to *in vivo* imaging, animals received the substrate D-luciferin (Biosynth) at 150 mg/kg in PBS by intraperitoneal injection and were anesthetized using 1–3% isoflurane (Abbott Laboratories, North Chicago, IL). Animals were placed onto a warmed stage inside the camera box and received continuous exposure to 1–2% isoflurane to sustain sedation during imaging. Imaging times ranged from 10 to 60 s, depending on the bioluminescence of the metastatic lesions. Five mice were imaged at a time. Tumor growth was monitored

Fig. 4. Antitumor activity of DACHPt-loaded micelle (DACHPt/m) prepared with PEG-*b*-P(Glu) 12–40 against s.c. C-26 tumor model ($n=5$). Saline(×); oxaliplatin at 6 mg/kg(△); 4 mg/kg(◇); 2 mg/kg(□). DACHPt-loaded micelle (DACHPt/m) 12–40 at 6 mg/kg(▲); 4 mg/kg(◆); 2 mg/kg(■). A. Tumor volume (mm^3) for oxaliplatin treatment; B. Relative body weight of mice for oxaliplatin treatment; C. Tumor volume (mm^3) for DACHPt/m treatment; D. Relative body weight of mice for DACHPt/m treatment. Data are expressed as averages±S.D. *Toxic death. **$p<0.001$.

by BLI every second day for 18 days. The light emitted from the bioluminescent tumors was detected *in vivo* by the IVIS Imaging System, was digitized and electronically displayed as a pseudocolor overlay onto a gray scale animal image. Regions of interest (ROI) from displayed images were drawn around the tumor sites and quantified as photons/second using the Living Image software. The statistical analysis of animal data was carried out by the unpaired *t*-test.

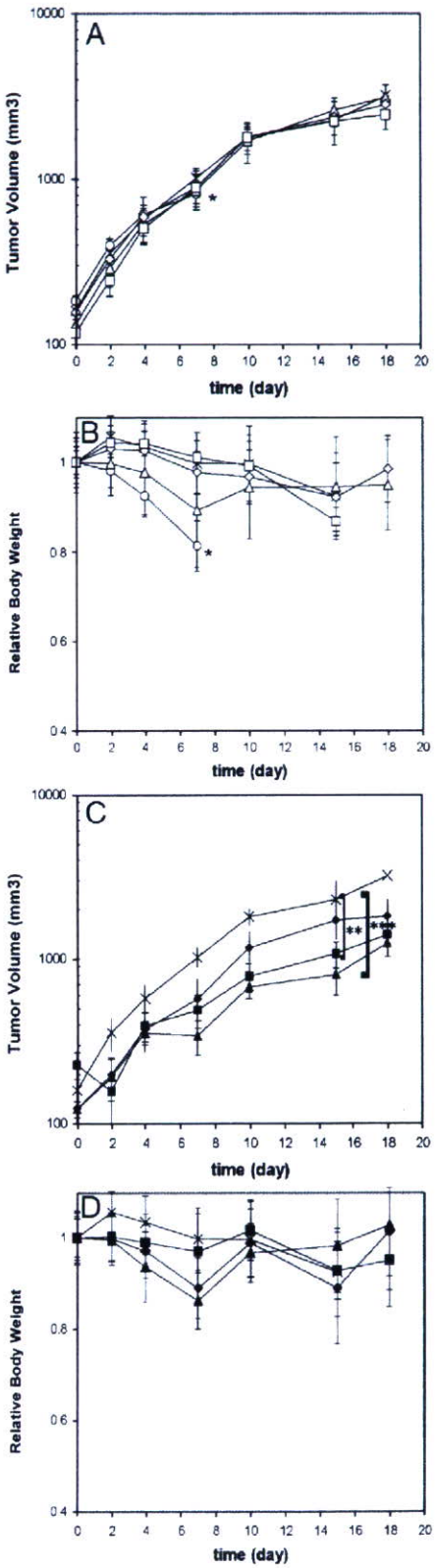

Fig. 5. Antitumor activity of DACHPt-loaded micelle (DACHPt/m) prepared with PEG-*b*-P(Glu) 12–20 against s.c. C-26 tumor model ($n=6$). Saline(×); oxaliplatin at 10 mg/kg(○); 6 mg/kg(△); 4 mg/kg(◇); 2 mg/kg(□). DACHPt-loaded micelle (DACHPt/m) 12–20 at 6 mg/kg(▲); 4 mg/kg(◆); 2 mg/kg(■). A. Tumor volume (mm^3) for oxaliplatin treatment; B. Relative body weight of mice for oxaliplatin treatment; C. Tumor volume (mm^3) for DACHPt/m treatment; D. Relative body weight of mice for DACHPt/m treatment. Data are expressed as averages ± S.D. *Toxic death. $^{**}p<0.01$. $^{***}p<0.005$.

3. Results

3.1. Micelle characterization

The metal-polymer complex formation between DACHPt and the carboxylic group of the p(Glu) in the PEG-*b*-P(Glu) led to the formation of narrowly distributed micellar assemblies (Fig. 1) with average diameters of approximately 40 nm (Table 1). The increase in the length of the p(Glu) block slightly enlarged the diameter of DACHPt/m (Table 1). The drug content in the micelles was determined to be remarkably high in all the micelle formulations (Table 1). The [DACHPt]/[Glu] molar ratios in DACHPt/m were found to be similar for all the formulations.

3.2. Biodistribution

3.2.1. Biodistribution of free oxaliplatin and DACHPt/m prepared with PEG-b-P(Glu) 12–40

The biodistribution study was performed on CDF_1 mice ($n=6$) bearing s.c. C-26 tumors. Oxaliplatin or DACHPt/m prepared with PEG-*b*-P(Glu) 12–40 were i.v. injected. In previous studies, DACHPt/m prepared with PEG-*b*-P(Glu) 12–40 have shown remarkably prolonged blood circulation, whereas free oxaliplatin was promptly removed from circulation. The Pt in plasma was determined to be 15% of the injected dose at 24 h post-injection, and more than 8% even at 48 h after injection for DACHPt/m [22]. This prolonged blood circulation of DACHPt/m was reasonably associated with the high kinetic stability of the micelles in phosphate buffered saline at 37 °C [22].

The accumulations of oxaliplatin and DACHPt/m in normal tissues (kidney, liver, spleen, and muscle) and solid tumor (C-26 cells) are shown in Fig. 2. Oxaliplatin was rapidly distributed to each organ in agreement with its rapid plasma clearance. In contrast, DACHPt/m showed cumulative accumulation in each organ and solid tumor ($p<0.001$) due to its remarkably prolonged blood circulation time, and the Pt level in the liver, spleen, and tumor continuously increased up to approximately 48 h after injection (Fig. 2). Consequently, the DACHPt/m exhibited 20-, 4-, and 25-fold higher accumulation in the liver, spleen, and tumor, respectively, than oxaliplatin at 48 h after injection. To assess the selectivity to the solid tumor, the